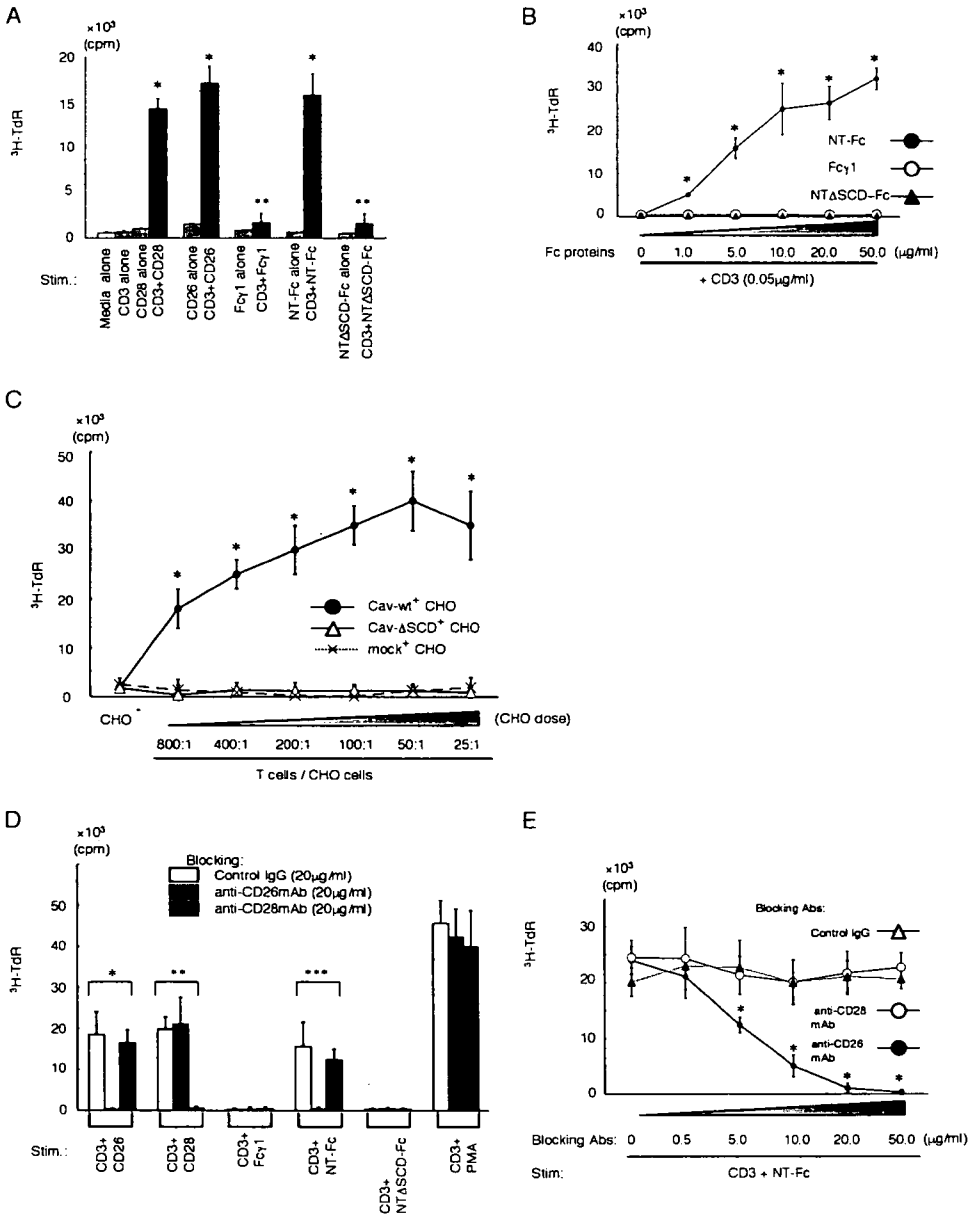

FIGURE 3. **NT-Fc is costimulatory with anti-CD3 for proliferation of peripheral blood T-cells.** *A*, purified T-cells were stimulated with immobilized antibodies and/or Fc fusion proteins (anti-CD3, 0.05 μg/ml; anti-CD28, anti-CD26, Fcγ1, NT-Fc, NTΔSCD-Fc, each at 5 μg/ml). Proliferation was measured by uptake of [^{3}H]TdR as described under "Experimental Procedures." Values shown are means ± S.E. of determinations from triplicate cultures of five independent donors. * shows points of significant increase ($p < 0.05$), whereas ** indicates points of no significant change compared with controls. *B*, purified T-cells were stimulated with immobilized Fc fusion proteins at indicated concentrations in the presence of immobilized anti-CD3 (0.05 μg/ml). Proliferation was measured as described in *A*. Values shown are means ± S.E. of determinations from triplicate cultures of five independent donors. * shows points of significant increase ($p < 0.05$) compared with control. *C*, purified T-cells were cultured in the presence of anti-CD3 (0.05 μg/ml) in solution, with varying amounts of CHO transfectants that were fixed with 0.05% glutaraldehyde. *Cav-wt⁺ CHO*, *Cav-ΔSCD⁺ CHO*, or *mock⁺ CHO* represent CHO cells stably transfected with GFP-full-length caveolin-1, GFP-caveolin-1 with the scaffolding domain deleted, or GFP expressing vector, respectively. Proliferation was measured as described in *A*. Values shown are means ± S.E. of determinations from triplicate cultures of five independent donors. * shows points of significant increase ($p < 0.05$) compared with control. *D*, following blocking with soluble anti-CD26, anti-CD28, or control mouse IgG, T-cells were stimulated, and proliferation was measured as described in *A*. Values shown are means ± S.E. of determinations from triplicate cultures of five independent donors. * and *** show results of significant inhibition obtained following blocking by anti-CD26 mAb ($p < 0.05$), and ** shows results of significant inhibition obtained following blocking by anti-CD28 mAb ($p < 0.05$). *E*, following incubation and blocking with increasing doses (0, 0.5, 5.0, 10.0, 20.0, and 50 μg/ml) of soluble anti-CD26 mAbs, anti-CD28 mAbs, or control mouse IgG, T-cells were stimulated by plate-bound anti-CD3 (0.05 μg/ml) plus NT-Fc (5 μg/ml), and proliferation was measured as described in *A*. Values shown are means ± S.E. of determinations from triplicate cultures of five independent donors. * shows points of significant decrease ($p < 0.05$) compared with controls.

T-cells were not stained with anti-CD26 mAb nor with NT-Fc (data not shown). These data suggested that the soluble N-terminal domain of caveolin-1 binds to cell surface CD26 and that the SCD of caveolin-1 is necessary for binding to CD26, as shown in our previous studies (14, 15).

To investigate the properties of binding of NT-Fc to CD26, we next examined the binding affinity with the Biacore system by injecting increasing concentrations of recombinant soluble CD26 (rsCD26) over each sensor surface containing recombinant Fc fusion proteins, Fcγ1, NT-Fc, or NTΔSCD-Fc (Fig. 2*C*). rsCD26 did not bind to control recombinant Fcγ1 on a Biacore sensor chip (*panel a* in Fig. 2*C*). For each concentration of rsCD26 injected, the binding response at equilibrium was calculated by subtracting the response observed in NT-Fc, resulting in a K_d value of $\sim 2 \times 10^{-5}$ M by equilibrium binding analysis (*panel b* in Fig. 2*C*). rsCD26 did not bind to NTΔSCD-Fc on a Biacore sensor chip (*panel c* in Fig. 2*C*). These results clearly indicated that the N-terminal domain of caveolin-1 binds directly to CD26.

We next evaluated whether NT-Fc stimulation had a similar effect as anti-CD26 mAb on CD26-mediated T-cell costimulation in J.CD26wt (13). As shown in Fig. 2*D*, IL-2 production of J.CD26wt induced by plate-bound anti-CD3 plus NT-Fc was observed to be at a similar level as that induced by anti-CD3 plus anti-CD28 or by anti-CD3 plus anti-CD26 (*, **, and *** in the *bar graph*), whereas IL-2 production was not observed in JKTwt (which is CD26-negative) following stimulation by anti-CD3 plus anti-CD26 nor by anti-CD3 plus NT-Fc (* and *** in Fig. 2*D*). IL-2 production by J.CD26wt or JKTwt was not observed with the use of control recombinant Fcγ1 nor NTΔSCD-Fc (# in Fig. 2*D*). To further investigate whether the T-cell costimulatory activity of NT-Fc was exerted via CD26, blocking experiments were

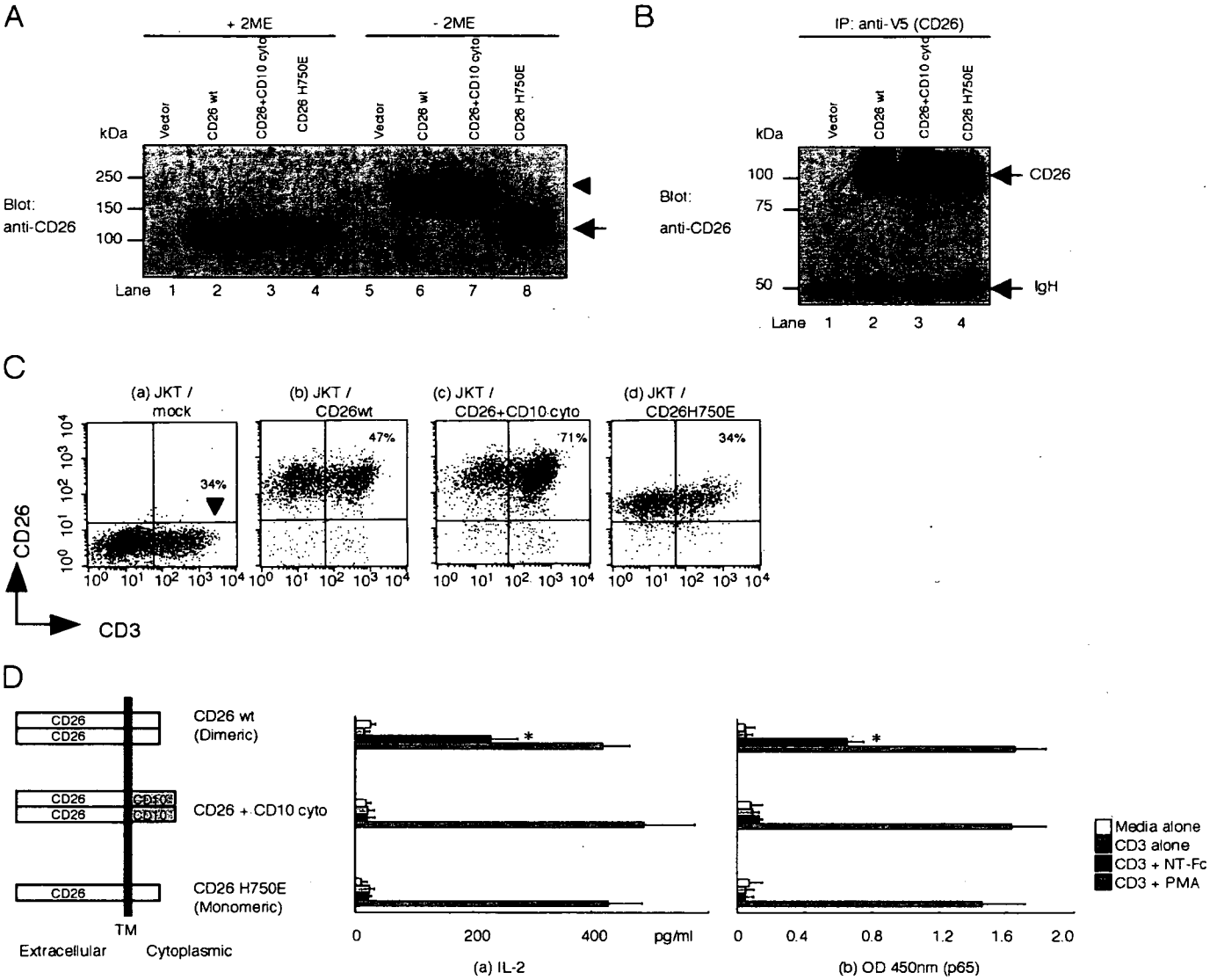

FIGURE 4. **The cytoplasmic tail of dimeric CD26 is necessary for anti-CD3 plus caveolin-1 costimulation.** *A*, Jurkat T-cells stably transfected with V5-tagged full-length CD26 (CD26wt), CD26-CD10 chimeric receptor (CD26 + CD10 cyto), or monomeric CD26 (CD26 H750E) were generated as described under "Experimental Procedures." Cell lysates were resolved in SDS-PAGE under reducing (*+2ME*) (*lanes 1–4*) or nonreducing (*−2ME*) conditions (*lanes 5–8*), and immunoblotted with anti-CD26 mAb. In nonreducing conditions, the *arrowhead* shows bands of dimeric CD26 (*lanes 6* and *7*), and the *arrow* indicates bands of monomeric CD26 (*lane 8*). *B*, cells were lysed and immunoprecipitated with anti-V5 mAb. IPs were resolved in 5–20% gradient SDS-PAGE under reducing conditions and immunoblotted with anti-CD26 mAb. *IgH* indicates immunoglobulin heavy chain. *C*, dot plots for expression of cell surface CD3 and CD26. % positive of CD3 is shown in mock vector-transfected Jurkat (*panel a*), and % positive of CD3 and CD26 is shown in other transfectants (*panels b–d*). *D*, Jurkat transfectants, which were stably transfected with full-length CD26 (CD26wt), CD26-CD10 chimeric receptor (CD26 + CD10 cyto), or CD26 containing mutation of histidine residue at amino acid 750 for glutamic acid (CD26 H750E), were stimulated with plate-bound anti-CD3 (1.0 μg/ml) in the presence or absence of plate-bound NT-Fc (10 μg/ml) or PMA (10 ng/ml). *Panel a*, following 48 h of culture, IL-2 concentration of the culture supernatant was measured by ELISA. Values shown are means ± S.E. of determinations from triplicate cultures. * shows points of significant increase ($p < 0.05$) compared with control. *Panel b*, Jurkat transfectants were stimulated as described in *panel a*, harvested for extraction of nuclear proteins, ad subjected to ELISA-based DNA-binding protein assay. Binding activity to p65 NF-κB component was revealed by absorbance value at 450 nm. Data represent mean ± S.E. from triplicate experiments. * shows a point of significant increase ($p < 0.05$).

conducted using CD26-specific mAb, which blocked binding of NT-Fc to J.CD26wt. As shown in Fig. 2*E*, IL-2 production induced by plate-bound anti-CD3 plus anti-CD26 was blocked by soluble anti-CD26 mAb but not by soluble anti-CD28 mAb (** and ##). In this experimental condition, IL-2 production induced by plate-bound anti-CD3 plus NT-Fc was blocked by soluble anti-CD26 mAb but not by soluble anti-CD28 mAb (* and # in Fig. 2*E*). Control Fγc1 or NTΔSCD-Fc did not have any T-cell costimulatory activity (Fig. 2*E*). Taken together, our results clearly indicated that caveolin-1 binds directly to CD26 and induces T-cell costimulation via CD26.

We next evaluated the ability of NT-Fc to reproduce the effects of anti-CD26 mAb on CD26-mediated T-cell costimulation (11, 35). As shown in Fig. 3*A*, T-cell proliferation induced by plate-bound anti-CD3 plus NT-Fc was observed to be at a similar level as that induced by anti-CD3 plus anti-CD28 or by anti-CD3 plus anti-CD26 (* in the *bar graph*), whereas T-cell proliferation was not observed using control recombinant Fcγ1 nor NTΔSCD-Fc (** in the *bar graph*). Moreover, T-cell costimulation induced by NT-Fc was observed in a dose-dependent manner, whereas increasing doses of Fcγ1 or NTΔSCD-Fc did not induce T-cell proliferation (Fig. 3*B*). To

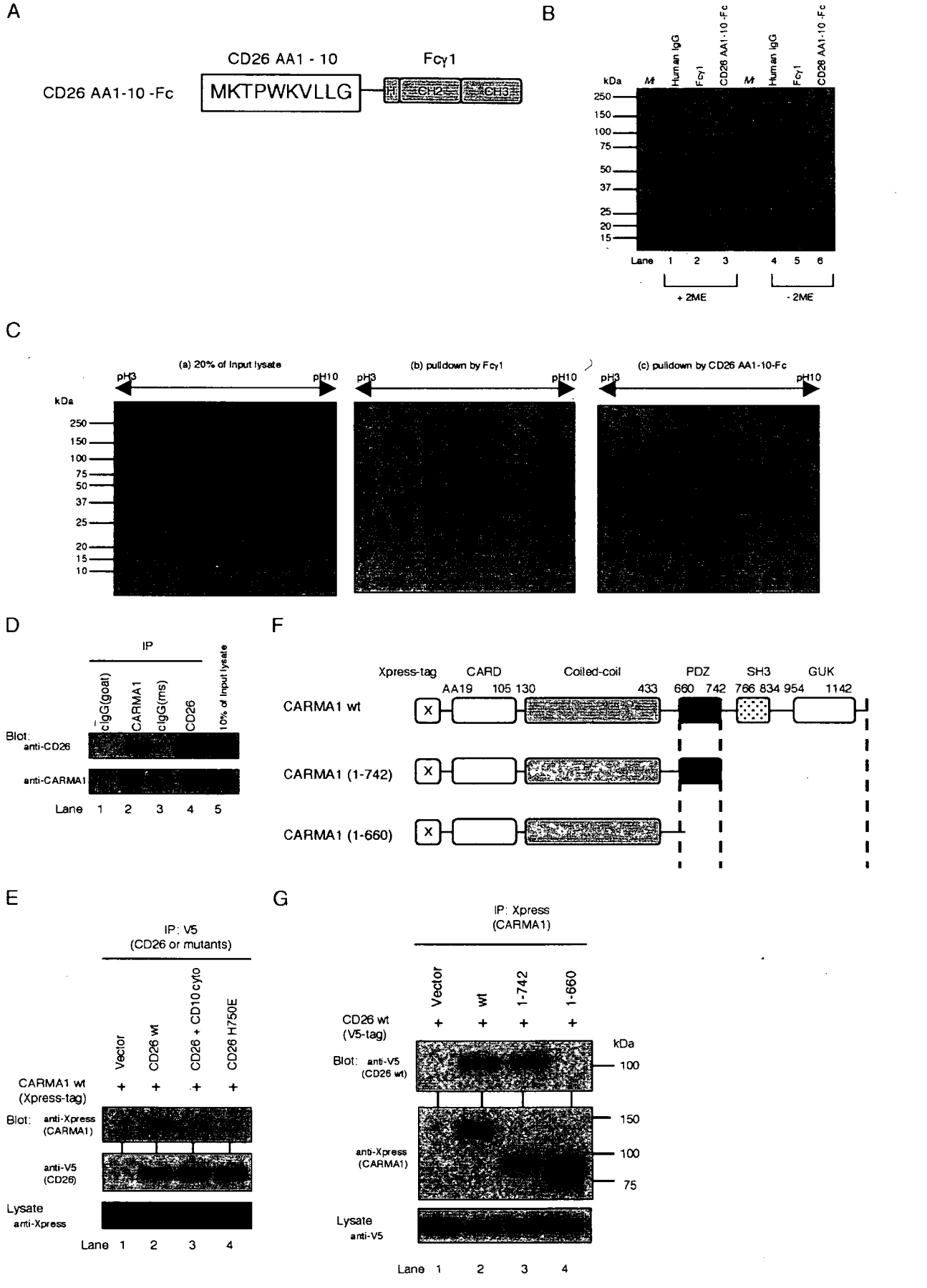
A
CD26 AA1 - 10
Fcγ1
CD26 AA1-10 -Fc
MKTPWKVLLG
H
CH2
CH3
B
kDa
M
Human IgG
Fcγ1
CD26 AA1-10-Fc
250
150
100
75
50
37
25
20
15
Lane 1 2 3 4 5 6
+ 2ME
- 2ME
C
(a) 20% of Input lysate
(b) pulldown by Fcγ1
(c) pulldown by CD26 AA1-10-Fc
pH3
pH10
kDa
250
150
100
75
50
37
25
20
15
10
D
IP
cIgG(goat)
CARMA1
cIgG(ms)
CD26
10% of Input lysate
Blot:
anti-CD26
anti-CARMA1
Lane 1 2 3 4 5
F
Xpress-tag
CARD
Coiled-coil
PDZ
SH3
GUK
AA19
105 130
433
660 742
766 834 954
1142
CARMA1 wt
CARMA1 (1-742)
CARMA1 (1-660)
X
E
IP: V5
(CD26 or mutants)
Vector
CD26 wt
CD26 + CD10 cyto
CD26 H750E
CARMA1 wt
(Xpress-tag)
+
Blot:
anti-Xpress
(CARMA1)
anti-V5
(CD26)
Lysate
anti-Xpress
Lane 1 2 3 4
G
IP: Xpress
(CARMA1)
Vector
wt
1-742
1-660
CD26 wt
(V5-tag)
kDa
Blot: anti-V5
(CD26 wt)
100
150
anti-Xpress
(CARMA1)
100
75
Lysate
anti-V5
Lane 1 2 3 4

further define the costimulatory activity of caveolin-1, we prepared CHO cells stably expressing human caveolin-1. As shown in Fig. 3*C*, we then showed that Cav-wt$^+$ CHO cells expressed T-cell costimulatory activity in the presence of anti-CD3 mAb, an effect not observed with mock$^+$ CHO cells nor Cav-ΔSCD$^+$ CHO cells. The costimulatory activity of Cav-wt$^+$ CHO cells was further observed in a cell number-dependent manner (* in Fig. 3*C*).

To further investigate whether the T-cell costimulatory activity of NT-Fc is exerted via CD26, blocking experiments were conducted using CD26-specific mAb which blocked binding of NT-Fc to J.CD26 (Fig. 2*B*). As shown in Fig. 3*D*, T-cell proliferation by plate-bound anti-CD3 plus anti-CD26 was blocked by soluble anti-CD26 mAb but not by soluble anti-CD28 mAb (*). On the other hand, T-cell proliferation by plate-bound anti-CD3 plus anti-CD28 was blocked by soluble anti-CD28 mAb but not by soluble anti-CD26 mAb (** in Fig. 3*D*). In this experimental condition, T-cell proliferation by plate-bound anti-CD3 plus NT-Fc was blocked by soluble anti-CD26 mAb but not by soluble anti-CD28 mAb (*** in Fig. 3*D*). Control Fγc1 or NTΔSCD-Fc did not have any T-cell costimulatory activity (Fig. 3*D*). Moreover, the blocking effect of CD26-specific mAb on NT-Fc costimulation was observed in a dose-dependent manner (* in Fig. 3*E*), and control IgG or anti-CD28 mAb at concentrations of 0–50 μg/ml did not block NT-Fc costimulation (Fig. 3*E*). Taken together with data shown in Figs. 1–3, these data suggested that NT-Fc functionally engages CD26 and not nonspecific proteins and that caveolin-1 has a costimulatory effect on T-cell proliferation via the TCR/CD3 pathway.

The proximal signaling molecules of CD26-mediated T-cell costimulation by caveolin-1 were next determined. We first examined whether the cytoplasmic tail of CD26 is responsible for T-cell costimulation by NT-Fc in the presence of anti-CD3 mAb. For this purpose, costimulation experiments were performed on Jurkat T-cells transfected with CD26-CD10 chimeric receptor. Moreover, whereas CD26 is reported to form homodimers on cell surface (36, 37), it remains to be determined whether dimeric CD26 is responsible for CD26-mediated T-cell costimulation. Therefore, costimulation experiments were conducted using Jurkat T-cells transfected with monomeric CD26 (CD26 H750E). We first verified the Jurkat-stable transfectants, as shown in Fig. 4*A*, and CD26wt, CD26 + CD10 cyto, and CD26 H750E were detected at ~100 kDa in reducing conditions (*lanes 2–4*), bands of CD26wt and CD26 + CD10 cyto migrated at ~200 kDa (*lanes 6* and *7*), and a band of CD26 H750E migrated at 100 kDa (*lane 8*) in nonreducing conditions, indicating that CD26wt and CD26 + CD10 cyto exist as dimers, and CD26 H750E exists as monomers in the Jurkat transfectants. Moreover, as shown in Fig. 4*B*, by immunoprecipitation using anti-V5 mAb, V5-tagged CD26 was detected by anti-CD26 mAb in each transfectant (CD26wt, CD26 + CD10 cyto, or CD26 H750E) in reducing SDS-PAGE (*lanes 2–4*). Furthermore, Fig. 4*C* showed the cell surface expression of CD3 and CD26 in Jurkat transfectants. CD3 was expressed at similar intensity among transfectants (*horizontal axis* of *panels a–d* in Fig. 4*C*), whereas the intensity of cell surface CD26 expression was different between CD26wt/CD26 + CD10 cyto and CD26 H750E (*vertical axis* of *panels b–d* in Fig. 4*C*), suggesting a difference between dimeric expression and monomeric expression. CD26 was not observed in mock vector-transfected Jurkat (*JKT/mock*; *panel a* in Fig. 4*C*). Using these Jurkat transfectants, costimulation experiments by NT-Fc were conducted. As shown in Fig. 4*D*, IL-2 production was observed in CD26wt-transfected Jurkat T-cells by stimulation with anti-CD3 plus NT-Fc (* in *panel a*), but not in CD26-CD10 chimera nor in CD26 H750E-transfected Jurkat. Moreover, p65, one of NF-κB components, was activated in CD26wt-transfected Jurkat T-cells following stimulation with anti-CD3 plus NT-Fc (* in *panel b*) but not in CD26-CD10 chimera nor in CD26 H750E-transfected Jurkat. Furthermore, IL-2 production or p65 induction by stimulation with anti-CD3 plus PMA was equally observed in either of CD26wt, CD26-CD10 chimera, or CD26 H750E transfected Jurkat (*panels a* and *b* of Fig. 4*D*). These data strongly suggested that the cytoplasmic tail of dimeric CD26, but not of monomeric CD26, is responsible for T-cell costimulation by NT-Fc in the presence of anti-CD3 mAb.

Because the cytoplasmic tail of CD26 appears to play a key role for CD26-mediated T-cell costimulation as shown in Fig. 4, we next explored signaling molecules associated with the cyto-

FIGURE 5. **The cytoplasmic tail of dimeric CD26 is associated with CARMA1.** *A*, schematic diagram of Fc fusion proteins of the cytoplasmic tail of CD26 (CD26 aa1–10). *MKTPWKVLLG* depicts amino acid residues of human CD26 at 1–10 positions. At the 3′ portion, the hinge (*H*) and CH2 and CH3 domains of human IgG_1 Fc are also indicated (*Fcγ1*). *B*, expressed fusion proteins were purified as described under "Experimental Procedures." Aliquots (5 μg) of control human IgG (*lanes 1* and *4*), Fcγ1 (*lanes 2* and *5*), and CD26 aa1–10-Fc (*lanes 3* and *6*) were subjected to SDS-PAGE under reducing (+*2ME*, *lanes 1–3*) or nonreducing (−*2ME*, *lanes 4–6*) conditions. Molecular weight markers are depicted in M_r. Proteins were visualized by staining with Coomassie Brilliant Blue. *C*, an aliquot (50 μg) of Jurkat lysates was separated by two-dimensional PAGE using pH 3.0–10 nonlinear (*NL*) IPG (isoelectric focusing of proteins using immobilized pH gradient) stripped in the first dimension and 4–12% SDS-PAGE, and the gels were stained with Coomassie Brilliant Blue (*panel a*). Aliquots (1 mg) of lysates were precleared by human IgG (2 μg) and proteins A-Sepharose, followed by immunoprecipitation with Fcγ1 (1 μg) (*panel b*) or CD26 aa1–10-Fc (1 μg) (*panel c*). IPs were analyzed by two-dimensional PAGE, and six spots were clearly detected in IP complex of CD26 aa1–10-Fc (*1–6* in *panel c*). * and ** were spots of Fcγ1 and CD26-Fc (aa1–10), respectively. Similar results were obtained in five independent experiments, and the panels shown are the representative results. *D*, J.CD26wt were lysed, and IP assays were conducted with anti-CARMA1 pAb (*goat*), anti-CD26 mAb (mouse (*ms*)), or control Ig (cIgG). IP complexes as well as 10% of input lysates were then separated using SDS-PAGE, immunoblotted with indicated antibodies. Similar results were obtained in three independent experiments. *E*, 293FT cells were transiently transfected with V5-tagged full-length CD26 (CD26wt), CD26-CD10 chimeric receptor (CD26 + CD10 cyto), or CD26 containing mutation of histidine residue at amino acid 750 for glutamic acid (CD26 H750E), together with Xpress-tagged full-length CARMA1 (CARMA1wt). Cells were lysed with TBSD buffer and immunoprecipitated with anti-V5 mAb. IPs were separated using 5–20% SDS-PAGE and immunoblotted with anti-Xpress mAb (*upper panel*), followed by stripping and reprobing with anti-V5 mAb (*lower panel*). Similar results were obtained in three independent experiments. *F*, schematic diagrams of Xpress-tagged CARMA1 and its deletion mutants: CARAM1wt, Xpress-tagged full-length CARMA1; CARMA1-(1–742), Xpress-tagged CARMA1 minus the SH3 + GUK domains; CARMA1-(1–660), Xpress-tagged CARMA1 minus the PDZ + SH3 + GUK domains. *G*, 293FT cells were transiently transfected with Xpress-tagged CARMA1wt, CARMA1 with the SH3 + GUK domains deleted (residues 1–742), or CARMA1 with the PDZ + SH3 + GUK domains deleted (residues 1–660), together with V5-tagged CD26wt. Cells were lysed with TBSD buffer and immunoprecipitated with anti-Xpress mAb. IPs were separated using SDS-PAGE and immunoblotted with anti-V5 mAb (*upper panel*), followed by stripping and reprobing with anti-Xpress mAb (*lower panel*). Similar results were obtained in three independent experiments.

plasmic tail of dimeric CD26. For this purpose, we prepared Fc fusion protein containing the first 10 aa of the N-terminal residues of CD26 (CD26 aa1–10-Fc) (Fig. 5*A*). As shown in Fig. 5*B*, purified protein of CD26 aa1–10-Fc was observed at ~37 kDa in reducing conditions (*lane 3*) and at ~70 kDa in nonreducing conditions (*lane 6*), suggesting that CD26 aa1–10-Fc formed homodimers. Following pulldown by CD26 aa1–10-Fc of Jurkat T-cell lysates, molecules that interacted with CD26 aa1–10-Fc were analyzed by two-dimensional SDS-PAGE. The gel of two-dimensional PAGE using input lysates is shown in Fig. 5*C* (*panel a*). Compared with two-dimensional gel analyzing IP complex by control Fcγ1 (*panel b* in Fig. 5*C*), six spots were detected by pulldown assays with CD26 aa1–10-Fc (*panel c* in Fig. 5*C*). Using matrix-assisted laser desorption ionization time-of-flight mass spectrometry, the proteins were determined to be as follows: spot 1, epidermal cytokeratin 2 (~66 kDa); spot 2, glutamyl-tRNA synthetase (~70 kDa); spot 3, tubulin (~50 kDa); spot 4, unnamed protein (~84 kDa); spot 5, CARMA1 (~120 kDa); or spot 6, HSP70 (~55 kDa), respectively (*panel c* in Fig. 5*C*). Following five independent repeats of these experiments with similar results, the unnamed protein (spot 4) was not identified more precisely by this procedure, and the other spots other than CARMA1 were ubiquitously expressed as housekeeping proteins. Therefore, CARMA1 was identified as an interacting protein with the cytoplasmic tail of CD26 and subjected to further examination.

For further confirmation, we next performed IP studies using lysates of J.CD26wt. As shown in Fig. 5*D*, CD26 was detected in a complex of lysates coprecipitated with anti-CARMA1 pAb (*lane 2* of *upper panel*), and not coprecipitated with control goat IgG (*lane 1* of *upper panel*). Moreover, CARMA1 was detected in a complex of lysates coprecipitated with anti-CD26 mAb (*lane 4* of *lower panel* in Fig. 5*D*), and not coprecipitated with control mouse IgG (*lane 3* of *lower panel* in Fig. 5*D*). These data suggested that CARMA1 binds to CD26 in cells. To determine the binding domain between CD26 and CARMA1, coimmunoprecipitation assay was next performed using 293FT-cells cotransfected with Xpress-tagged human full-length CARMA1 (CARMA1wt) and with CD26wt, CD26 + CD10 cyto, or CD26 H750E. As shown in Fig. 5*E*, CARMA1 was coprecipitated with CD26wt (*lane 2*) but not with CD26 + CD10 cyto nor CD26 H750E (*lanes 3* and *4*). These data strongly suggested that the cytoplasmic tail and dimerization of CD26 are necessary to interact with CARMA1. We next explored the binding domain of CARMA1 to CD26. For this purpose, we prepared the C-terminal truncated deletion mutants of CARMA1 (Fig. 5*F*). As shown in Fig. 5*G*, CD26 was coprecipitated with CARMA1wt or with CARMA1-(1–742) (*lanes 2* and *3*) but not with CARMA1-(1–600) (*lane 4*), suggesting that the PDZ domain in CARMA1 was necessary for binding to CD26.

To explore the role of CARMA1 in CD26-mediated T-cell costimulation, we used CARMA1-deficient Jurkat T-cell lines JPM50.6 to conduct rescue experiments (18). As shown in Fig. 6*A*, CARMA1 and CD26 were not detected in JPM50.6 (*lane 3* of *upper* and *lower panels*), whereas CARMA1 was expressed in native Jurkat and J.CD26wt (*lanes 1* and *2* of *lower panel*), and CD26 was expressed in J.CD26wt (*lane 2* of *upper panel*) but not in native Jurkat (*lane 1* of *upper panel*). We next generated the stable transfectants using JPM50.6 as described under "Experimental Procedures." Fig. 6*B* shows that transfected Xpress-tagged CARMA1 was expressed in JPM50.6/CARMA1wt, JPM50.6/CD26wt + CARMA1wt, and JPM50.6/CD26wt + CARMA1-(1–660) and that transfected V5-tagged CD26 was expressed in JPM50.6/CD26wt, JPM50.6/CD26wt + CARMA1wt, and JPM50.6/CD26wt + CARMA1-(1–660). Fig. 6*C* shows the cell surface expression of CD3 and CD26 in JPM50.6 transfectants. CD3 was expressed at similar intensity among transfectants (*horizontal axis* of *panels a–e* in Fig. 6*C*). Although the intensity of cell surface CD26 expression was similar among JPM50.6/CD26wt, JPM50.6/CD26wt + CARMA1wt, and JPM50.6/CD26wt + CARMA1-(1–660) (*panels b, d,* and *e* in Fig. 6*C*), CD26 was not observed in JPM50.6/V (mock vector) and JPM50.6/CARMA1wt (*panels a* and *c* in Fig. 6*C*). Using these transfectants, IL-2 production and NF-κB activation assays were performed with stimulation by anti-CD3 alone or anti-CD3 plus NT-Fc. As shown in Fig. 6*D*, IL-2 production induced by anti-CD3 plus NT-Fc was clearly observed in JPM50.6/CD26wt + CARMA1 but not in JPM50.6, JPM50.6/CD26wt, JPM50.6/CARMA1, nor JPM50.6/CD26wt + CARMA1-(1–660) (*panel a*). Similarly, NF-κB activation induced by anti-CD3 plus NT-Fc was clearly observed in JPM50.6/CD26wt + CARMA1 but not in JPM50.6, JPM50.6/CD26wt, JPM50.6/CARMA1, nor JPM50.6/CD26wt+ CARMA1-(1–660) (*panel b* in Fig. 6*D*). Furthermore, IL-2 production or NF-κB activation by stimulation with anti-CD3 plus PMA was equally observed in either of the transfectants (*panels a* and *b* of Fig. 6*D*). Taken together, these results suggested that CARMA1 is necessary to exert CD26-mediated costimulation by NT-Fc.

As shown above, costimulation of CD26 is observed to be exerted via interaction of CD26 with CARMA1 in the cytoplasm in Jurkat cells. To confirm this interaction more profoundly, we performed biochemical assays using human T-cells purified from healthy adult peripheral blood mononuclear cells (APB-T-cells). For this purpose, we first conducted IP studies using lysates of APB-T-cells. As shown in Fig. 7*A*, CD26 was detected in a complex of lysates coprecipitated with anti-CARMA1 pAb (*lane 2* of *upper panel*), and not coprecipitated with control goat IgG (*lane 1* of *upper panel*). Moreover, CARMA1 was detected in a complex of lysates coprecipitated with anti-CD26 mAb (*lane 4* of *lower panel* in Fig. 7*A*), and not coprecipitated with control mouse IgG (*lane 3* of *lower panel* in Fig. 7*A*). These data suggested that CARMA1 binds to CD26 in normal T-cells.

We previously showed that nonactivated peripheral blood T-cells treated with the anti-CD26 mAb 1F7 resulted in CD26 recruitment to lipid rafts, concomitant with increased tyrosine phosphorylation of ZAP70, $p56^{lck}$, and TCRζ (33). Other investigators have reported that in the process of activation of NF-κB via CD3 costimulation, CARMA1 was recruited to lipid rafts along with Bcl10 and IKKβ (18, 25, 27, 38, 39). We therefore examined whether CD26 and CARMA1 are recruited to lipid rafts by anti-CD3 plus caveolin-1 costimulation in normal T-cells. For this purpose, using a sucrose gradient separation method, we prepared lipid raft

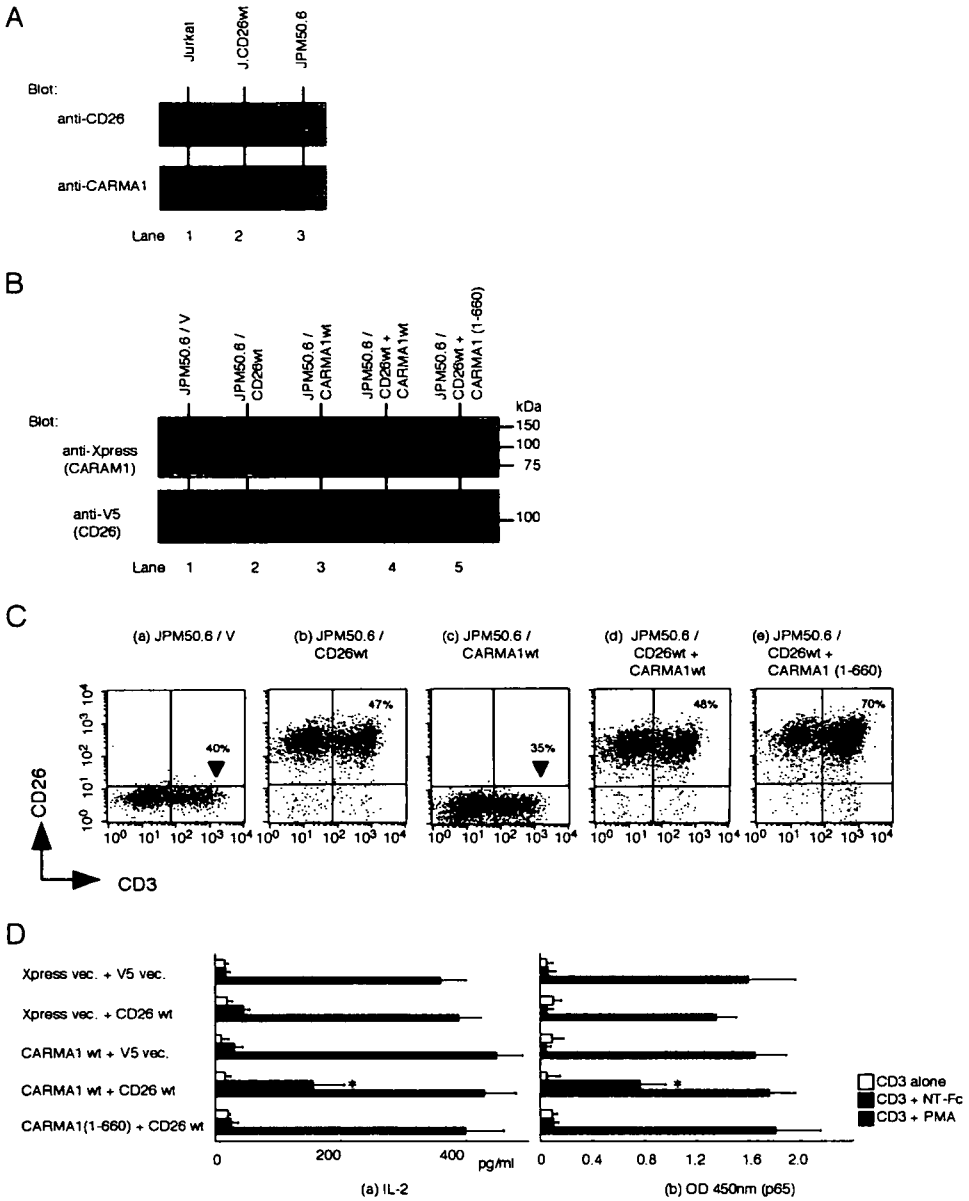

FIGURE 6. **CARMA1 is necessary for CD26-mediated costimulation by caveolin-1.** *A*, cell lysates of native Jurkat, J.CD26wt, or JPM50.6 were resolved in SDS-PAGE under reducing conditions, followed by immunoblotting with anti-CD26 mAb (*upper panel*) or anti-CARMA1 pAb (*lower panel*). *B*, JPM50.6 cells stably transfected with V5-tagged full-length CD26 (CD26wt) and/or Xpress-tagged full-length CARMA1 (CARMA1wt) or CARMA1 with the PDZ + SH3 + GUK domains deleted (CARMA1-(1–660)) were generated as described under "Experimental Procedures." Lysates were resolved in SDS-PAGE and immunoblotted with anti-Xpress mAb (CARMA1) (*upper panel*) or anti-V5 mAb (CD26) (*lower panel*). *C*, dot plots for cell surface expression of CD3 and CD26. % positive of CD3 is shown in mock vector-transfected JPM (*panel a*) and CARMA1-transfected JPM 50.6 (*panel c*), and % positive of CD3 and CD26 is shown in other transfectants (*panels b, d,* and *e*). *D*, JPM50.6 transfectants, which were described in *B*, were stimulated with plate-bound anti-CD3 in the presence or absence of plate-bound NT-Fc as described in Fig. 4*D*. *Panel a*, following 48 h of culture, IL-2 concentration of the culture supernatant was measured by ELISA. Values shown are means ± S.E. of determinations from triplicate cultures. * shows points of significant increase ($p < 0.05$) compared with control. *Panel b*, JPM50.6 transfectants were stimulated as described in *panel a* and harvested for nuclear extract. Each 5 μg of nuclear extract was subjected to ELISA-based DNA-binding protein assay. Binding activity to p65 NF-κB component was revealed by absorbance value at 450 nm. Data represent mean ± S.E. from triplicate experiments. * shows a point of significant increase ($p < 0.05$). *Xpress vec.* or *V5 vec.* depicts pcDNA4/HisMax or pEF6/V5 empty vector as a mock, respectively.

fractions of APB-T-cell lysates in the presence or absence of anti-CD3 plus NT-Fc costimulation. As shown in Fig. 7*B*, following stimulation with anti-CD3 plus NT-Fc, CD26, CARMA1, Bcl10, and IKKβ were detected in the lipid raft fractions, whereas CD26, CARMA1, Bcl10, and IKKβ were not detected in the lipid raft fractions after stimulation with anti-CD3 alone. Moreover, time course analysis revealed that CD26, CARMA1, Bcl10, and IKKβ were migrated into lipid rafts after stimulation with anti-CD3 plus NT-Fc (Fig. 7*C*), whereas CD26, CARMA1, Bcl10, and IKKβ were not detected after anti-CD3 treatment (data not shown). Furthermore, to examine whether CD26 and CARMA1 forms a complex with Bcl10 and IKKβ in lipid rafts, coprecipitation assay was performed using lipid raft fractions of APB-T-cell lysates from cells costimulated with anti-CD3 plus NT-Fc. As shown in Fig. 7*D*, CD26, CARMA1, Bcl10, and IKKβ in lipid rafts were coprecipitated with CD26 (*lane 4*), although not detected in the lysates of APB-T-cells following stimulation with anti-CD3 alone (*lane 2*). Taken together, these data indicated that ligation of CD26 by caveolin-1 recruits a complex of CARMA1, Bcl10, and IKKβ to lipid rafts in normal T-cells.

To examine the role of CARMA1 on CD26-mediated T-cell costimulation more directly, we performed siRNA experiments in freshly isolated APB-T-cells. For this purpose, we prepared two sets of specific siRNA against CARMA1 as described under "Experimental Procedures," and both of these siRNAs decreased CARMA1 expression in APB-T-cells, whereas the expression levels of CD26, TCR-β, or β-actin were not changed in the presence of control siRNA, ss1-siRNA, or ss2-siRNA (*inside box* of Fig. 7*E*). After transfection of these siRNAs into APB-T-cells, the proliferation assay was performed in the presence of anti-CD3 plus NT-Fc stimulation. As shown in Fig. 7*E*, T-cell proliferation stimulated with anti-CD3 plus NT-Fc was decreased in T-cells treated with siRNAs against CARMA1, whereas T-cell proliferation was observed in T-cells treated with control siRNA (* in Fig. 7*E*). Moreover, T-cell proliferation stimulated with anti-CD3 plus PMA was observed in either of control siRNA, ss1- or ss2-siRNA (** in Fig. 7*E*). These results suggested that CARMA1 plays an important role in signal transduction following CD26 binding to caveolin-1, leading to T-cell proliferation in normal T-cells.

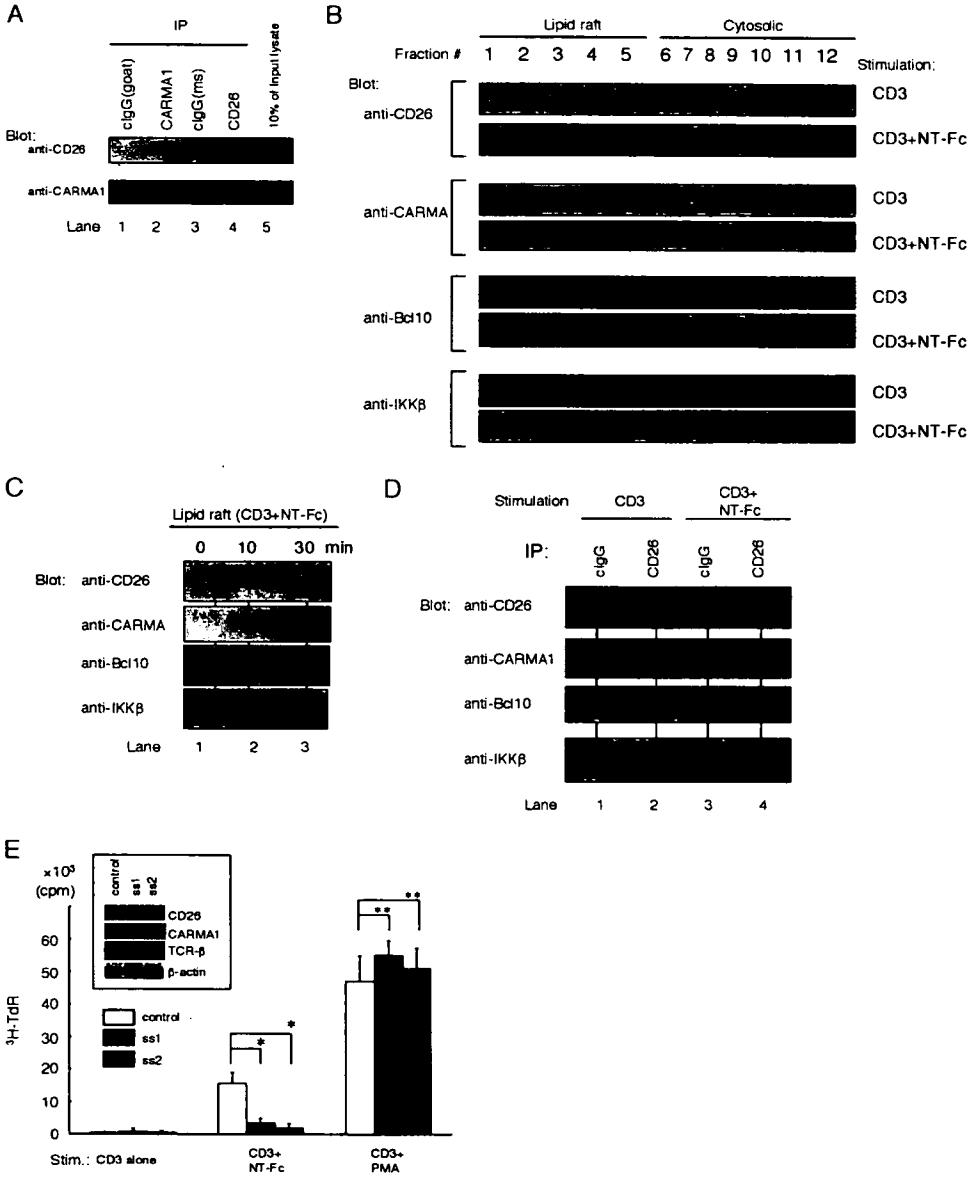

FIGURE 7. **CARMA1 plays an important role in CD26-mediated costimulation by caveolin-1 in human peripheral blood T-cells.** *A*, purified T-cells were lysed, and IP assays were conducted with anti-CARMA1 pAb (*goat*), anti-CD26 mAb (mouse (*ms*)), or control Ig (*cIgG*). IP complexes as well as 10% of input lysates were then separated using SDS-PAGE and immunoblotted with the indicated antibodies. Similar results were obtained in three independent experiments. *B*, purified T-cells were stimulated for 10 min with anti-CD3 alone (0.05 μg/ml) or with anti-CD3 plus NT-Fc (5.0 μg/ml), and lysates were prepared by sucrose gradient centrifugation as described under "Experimental Procedures." The distribution of CD26, CARMA1, Bcl10, and IKKβ was determined by immunoblotting with specific antibodies. Similar results were obtained in three independent experiments. *C*, purified T-cells were stimulated for 0, 10, and 30 min with anti-CD3 plus NT-Fc, and lysates were prepared by sucrose gradient centrifugation as described under "Experimental Procedures." The distribution of CD26, CARMA1, Bcl10, and IKKβ was determined by immunoblotting with specific antibodies. Similar results were obtained in three independent experiments. *D*, purified T-cells were stimulated with anti-CD3 alone (*lanes 1* and *2*) or with anti-CD3 plus NT-Fc (*lanes 3* and *4*), and lipid raft fractions were prepared as described in *A*, and immunoprecipitation of lipid rafts with control IgG (cIgG) (*lanes 1* and *3*) or anti-CD26 mAb (*lanes 2* and *4*) was performed as described under "Experimental Procedures." IPs were resolved in SDS-PAGE and immunoblotted with indicated antibodies. Similar results were obtained in three independent experiments. *E*, purified T-cells were transfected with sense-siRNA (ss1 and ss2) of CARMA1 gene or mismatched siRNA (*control*) using HVJ-E vector. Cell lysates were resolved by SDS-PAGE and immunoblotted with indicated antibodies, followed by stripping and reprobing with anti-β-actin antibody (*inside box*). Purified T-cells treated with siRNA were stimulated and subjected to T-cell proliferation assay as described in Fig. 3*A*. Values shown are means ± S.E. of determinations from triplicate cultures of five independent donors. * shows points of significant decrease ($p < 0.05$), and ** indicates points of no significant change compared with controls.

DISCUSSION

In this study, we showed that caveolin-1 is the costimulatory ligand for CD26, and that ligation of CD26 by caveolin-1 induces T-cell proliferation and NF-κB activation with costimulation of TCR/CD3. Moreover, we showed that the cytoplasmic tail of CD26 in T-cell interacts with CARMA1, resulting in signal transduction leading to NF-κB activation and that ligation of CD26 by caveolin-1 recruits a complex of CD26, CARMA1, Bcl10, and IKKβ to lipid rafts.

Enhancement of CD26 expression in autoimmune diseases may correlate with disease severity (40, 41), because patients with autoimmune diseases such as Grave's disease and rheumatoid arthritis have increased levels of CD26 + T-cells in their peripheral blood as well as inflamed tissues, including thyroid and synovial fluids and membranes (9, 42). These findings imply that CD26 + T-cells play a role in the inflammation process and subsequent tissue destruction. Originally characterized as a T-cell activation antigen, human CD26 is preferentially expressed on the CD4+ memory T-cell subset and is up-regulated after T-cell activation (2, 3, 10). Along with its enhanced expression on activated T-cells, various lines of evidence have converged to demonstrate that CD26 is functionally associated with T-cell signal transduction processes relating to T-cell activation (2, 10, 11, 43). However, the precise mechanism involved in T-cell activation via CD26 in response to memory antigen such as tetanus toxoid remains to be clearly characterized, including the identification of its costimulatory ligand and the associated proximal signaling molecules. Recently, we demonstrated that CD26 binds to caveolin-1 on APC and that residues 201–211 of CD26 along with the serine catalytic site at residue 630, which constitute a pocket structure of CD26/DPPIV, contribute to binding to the caveolin-1 scaffolding domain (14). This region in CD26 contains a caveolin-binding domain ($\Phi X\Phi XXXX\Phi XX\Phi$; Φ and X depict aromatic residue and any amino acid, respectively), specifically WVYEEEVFSAY in CD26 (2, 44). These

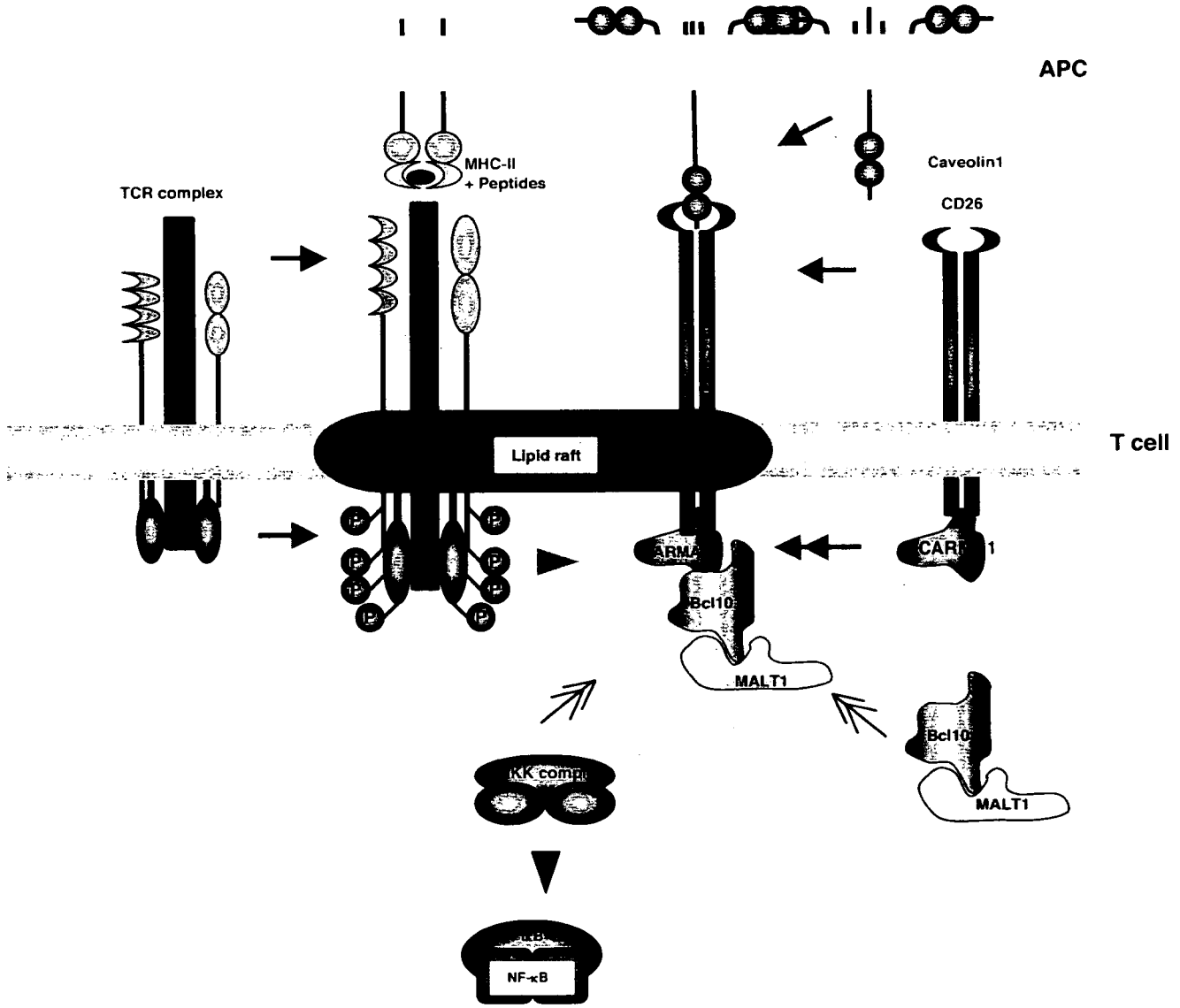

FIGURE 8. **A model for signaling by TCR and CD26 costimulation.** Stimulation of cells through TCR complexes leads to phosphorylation of cytoplasmic immunoreceptor tyrosine-based activation motifs by ligation of peptide-loaded major histocompatibility complex class II (*bold arrows*) and recruitment and activation of phosphatidylinositol 3-kinase and PKCθ (*gray arrowhead*). Meanwhile, caveolin-1, of which the N-terminal extracellular regions are presented on antigen-loaded APC, ligates CD26, which exists as dimers on the cell surface and recruits lipid rafts (*gray arrows*) while interacting with CARMA1 (*gray double-headed arrow*). The recruitment of CARMA1 along with CD26 to lipid rafts also recruits the CARMA1-Bcl10-IKKs complex (*black double-headed arrows*), leading to activation of the IKK complex (*black double-headed arrows*) and finally activation of NF-κB.

observations strongly support the notion that DPPIV enzyme activity is necessary to exert T-cell costimulatory activation via CD26 as demonstrated in our previous report using CD26 specific mAbs (13).

To examine the binding of caveolin-1 to CD26 in T-cells, we used soluble Fc fusion proteins containing the N-terminal domain of caveolin-1 (NT-Fc) (Fig. 1), and we found that NT-Fc binds specifically to CD26 to induce T-cell proliferation in the presence of TCR/CD3 costimulation (Figs. 2 and 3). Moreover, the binding affinity between caveolin-1 and CD26 ($K_d \sim 2 \times 10^{-5}$ M), as determined by the Biacore system (Fig. 2*C*), is comparable with that of other costimulatory molecules with important roles in immune responses and their associated ligands, such as CD2-CD5 ($K_d \sim 10^{-6}$ M), CD80-CD28 ($K_d \sim 10^{-7}$ M), and CD86-CD28 ($K_d \sim 10^{-6}$ M) (45–47). Until now, CD26-mediated T-cell costimulation was performed using anti-CD26 mAbs, resulting in various CD26 functions (4, 7, 48, 49). Assuming that the affinity between antigen and antibody is higher ($K_d \sim 10^{-9}$ M) than that of a ligand-receptor system, and that ligand-specific conformations are capable of differentially activating distinct signaling partners (50), ligand-dependent pathways may be predicted to have different signals associated with the antigen-antibody system and ligand-receptor system.

We have demonstrated previously that ligation of CD26 by the anti-CD26 mAb 1F7 induces T-cell costimulation and IL-2 production by CD26-transfected Jurkat T-cell lines, while increasing tyrosine phosphorylation of signaling molecules such as ZAP70, p56^{lck}, and CD3ζ was observed (2, 7, 12). In addition, we have shown that ligation of the CD26 molecules by the anti-CD26 mAb 1F7 increases the recruitment of CD26 molecules with CD45RO to lipid rafts, resulting in increased tyrosine phosphorylation of signaling molecules (33). However,

the precise proximal signaling pathway of CD26 has not yet been identified, particularly in view of the fact that the cytoplasmic tail of CD26 contains only 6 amino acid residues without a common signaling motif structure. Moreover, it has been unclear whether the short cytoplasmic tail is responsible for signal transduction associated with CD26-mediated costimulation. In this study, using recombinant CD26-CD10 chimeric receptor, we showed that the cytoplasmic tail of CD26 is indeed responsible for T-cell costimulation induced by anti-CD3 plus caveolin-1 (Fig. 4*D*). Furthermore, to explore the proximal signaling molecules interacting with the cytoplasmic tail of dimeric CD26, we used proteomic analyses with Fc fusion proteins containing the cytoplasmic amino acid residues of CD26 (Fig. 5, *A* and *B*) to identify that CARMA1 binds to the cytoplasmic tail of dimeric CD26 (Fig. 5*C*). Moreover, we demonstrated here that a PDZ domain in CARMA1 is necessary for binding to CD26 (Fig. 5*G*). The importance of CARMA1 in CD26-mediated costimulation is also shown by rescue experiments using the CARMA1-deficient Jurkat T-cell line JPM50.6 (Fig. 6*D*) and using siRNA against CARMA1 in APB-T-cells (Fig. 7*E*). CARMA1, containing caspase-recruitment domain and MAGUK domains, plays an essential role in the NF-κB activation and IL-2 expression induced by CD3-CD28 or CD28-PMA stimulation (18, 22). After being phosphorylated, CARMA1 functions as a signaling intermediate downstream of PKCθ and upstream of IKK in the TCR signaling transduction pathway leading to NF-κB activation (39, 51). Because MAGUK domain-containing proteins are generally involved in the organization of multiprotein complexes at the interface of the cytoplasmic membrane (52), it is possible that CARMA1 associates with as yet undefined membrane proteins in the immunological synapse of T-cells. In this regard, our present data suggest a novel mechanism for CAMRA1 function as it complexes with Bcl10 and IKK to transduce CD26-costimulatory signals. Moreover, as shown Fig. 5*C*, cytoskeletal proteins were also observed in the complex in the pulldown assays with CD26 aa1–10-Fc. Because MAGUK domain-containing proteins are generally involved in the organization of multiprotein complexes in the cytoskeleton (52), the downstream signaling of CD26 may also be associated with cytoskeletal assembly via CARMA1. The association of CD26, CARMA1, and the cytoskeleton will be elucidated in future studies.

CD26/DDPIV is reported to exist as homodimers, a structural organization that allows access of substrates to DPPIV catalytic activity (36, 37). Although DPPIV activity is crucial for CD26-mediated T-cell costimulation (13, 30), the exact role played by DPPIV in this process is unclear. Our previous study showed that the enzymatic pocket structure of the DPPIV catalytic site is necessary for binding of CD26 to caveolin-1, leading to the up-regulation of CD86 expression on APC (14, 15). In this study, we found that monomeric CD26 H750E, which has a 300-fold decrease in catalytic activity (36), does not bind to CARMA1 (Fig. 5*E*), resulting in loss of CD26-mediated T-cell costimulation by anti-CD3 plus caveolin-1 (Fig. 4*D*). Therefore, dimerization of CD26 is not only necessary for binding to caveolin-1 but also serves as a scaffolding structure for the cytoplasmic signaling molecule CARMA1. The precise binding position of CARMA1 in the cytoplasmic domain of CD26 remains to be elucidated in future work, because PDZ domains bind primarily to specific C-terminal motifs (X(S/T)X(V/L), where X depicts any amino acid) or internal target motifs as well as other PDZ domains (52).

Based upon this study, we propose the following model to explain the sequence of events leading from CD26-CD3 costimulation to NF-κB activation (Fig. 8). In CD3-CD26 costimulation, TCR engagement by peptide-loaded major histocompatibility complex class II presented on APC activates phosphatidylinositol 3-kinase via phosphorylation of immunoreceptor tyrosine-based activation motifs in TCR, leading the recruitment of PKCθ and IKK complex in lipid rafts (16, 18, 25, 38). Concomitantly, CD26 ligation by caveolin-1 on APC recruits CD26-interacting CARMA1 to lipid rafts, resulting in the formation of a CARMA1-Bcl10-MALT1-IKK complex, and this membrane-associated Bcl10 complex then activates IKK through ubiquitination of the NF-κB essential modulator. This study involving Jurkat T-cell lines and human peripheral T-cells represents a different cellular system than those with murine T-cells, where other investigators previously described a role for CD26 in thymic development of murine T-cells (53, 54). Our objective with this study was to define a costimulatory ligand for CD26 and proximal signaling molecule of CD26 in human T-cells, with a future aim of analyzing the *in vivo* role of CD26-mediated T-cell immunity.

In conclusion, we have now demonstrated that CD26 on the T-cell surface binds to caveolin-1, hence identifying the first endogenously expressed CD26 costimulatory ligand in the immune system. Moreover, the caveolin-1-CD26 interaction results in strong T-cell costimulation as a result of the recruitment of a molecular complex consisting of CARMA1-Bcl10-MALT1-IKK in lipid rafts. Our findings will therefore serve as a foundation for future insights into the regulation of T-cell costimulation via the CD26 molecule.

REFERENCES

1. Nanus, D. M., Engelstein, D., Gastl, G. A., Gluck, L., Vidal, M. J., Morrison, M., Finstad, C. L., Bander, N. H., and Albino, A. P. (1993) *Proc. Natl. Acad. Sci. U. S. A.* **90,** 7069–7073
2. Tanaka, T., Camerini, D., Seed, B., Torimoto, Y., Dang, N. H., Kameoka, J., Dahlberg, H. N., Schlossman, S. F., and Morimoto, C. (1992) *J. Immunol.* **149,** 481–486
3. Fox, D. A., Hussey, R. E., Fitzgerald, K. A., Acuto, O., Poole, C., Palley, L., Daley, J. F., Schlossman, S. F., and Reinherz, E. L. (1984) *J. Immunol.* **133,** 1250–1256
4. De Meester, I., Korom, S., Van Damme, J., and Scharpe, S. (1999) *Immunol. Today* **20,** 367–375
5. Fleischer, B. (1994) *Immunol. Today* **15,** 180–184
6. Kahne, T., Lendeckel, U., Wrenger, S., Neubert, K., Ansorge, S., and Reinhold, D. (1999) *Int. J. Mol. Med.* **4,** 3–15
7. Morimoto, C., and Schlossman, S. F. (1998) *Immunol. Rev.* **161,** 55–70
8. von Bonin, A., Steeg, C., Mittrucker, H. W., and Fleischer, B. (1997) *Immunol. Lett.* **55,** 179–182
9. Eguchi, K., Ueki, Y., Shimomura, C., Otsubo, T., Nakao, H., Migita, K., Kawakami, A., Matsunaga, M., Tezuka, H., and Ishikawa, N. (1989) *J. Immunol.* **142,** 4233–4240
10. Morimoto, C., Torimoto, Y., Levinson, G., Rudd, C. E., Schrieber, M., Dang, N. H., Letvin, N. L., and Schlossman, S. F. (1989) *J. Immunol.* **143,** 3430–3439
11. Dang, N. H., Torimoto, Y., Deusch, K., Schlossman, S. F., and Morimoto, C. (1990) *J. Immunol.* **144,** 4092–4100
12. Hegen, M., Kameoka, J., Dong, R. P., Schlossman, S. F., and Morimoto, C.

(1997) *Immunology* **90,** 257–264
13. Tanaka, T., Kameoka, J., Yaron, A., Schlossman, S. F., and Morimoto, C. (1993) *Proc. Natl. Acad. Sci. U. S. A.* **90,** 4586–4590
14. Ohnuma, K., Yamochi, T., Uchiyama, M., Nishibashi, K., Yoshikawa, N., Shimizu, N., Iwata, S., Tanaka, H., Dang, N. H., and Morimoto, C. (2004) *Proc. Natl. Acad. Sci. U. S. A.* **101,** 14186–14191
15. Ohnuma, K., Yamochi, T., Uchiyama, M., Nishibashi, K., Iwata, S., Hosono, O., Kawasaki, H., Tanaka, H., Dang, N. H., and Morimoto, C. (2005) *Mol. Cell. Biol.* **25,** 7743–7757
16. Egawa, T., Albrecht, B., Favier, B., Sunshine, M. J., Mirchandani, K., O'Brien, W., Thome, M., and Littman, D. R. (2003) *Curr. Biol.* **13,** 1252–1258
17. Hara, H., Wada, T., Bakal, C., Kozieradzki, I., Suzuki, S., Suzuki, N., Nghiem, M., Griffiths, E. K., Krawczyk, C., Bauer, B., D'Acquisto, F., Ghosh, S., Yeh, W. C., Baier, G., Rottapel, R., and Penninger, J. M. (2003) *Immunity* **18,** 763–775
18. Wang, D., You, Y., Case, S. M., McAllister-Lucas, L. M., Wang, L., DiStefano, P. S., Nunez, G., Bertin, J., and Lin, X. (2002) *Nat. Immun.* **3,** 830–835
19. Bertin, J., Wang, L., Guo, Y., Jacobson, M. D., Poyet, J. L., Srinivasula, S. M., Merriam, S., DiStefano, P. S., and Alnemri, E. S. (2001) *J. Biol. Chem.* **276,** 11877–11882
20. Gaide, O., Martinon, F., Micheau, O., Bonnet, D., Thome, M., and Tschopp, J. (2001) *FEBS Lett.* **496,** 121–127
21. Che, T., You, Y., Wang, D., Tanner, M. J., Dixit, V. M., and Lin, X. (2004) *J. Biol. Chem.* **279,** 15870–15876
22. Gaide, O., Favier, B., Legler, D. F., Bonnet, D., Brissoni, B., Valitutti, S., Bron, C., Tschopp, J., and Thome, M. (2002) *Nat. Immun.* **3,** 836–843
23. Hara, H., Bakal, C., Wada, T., Bouchard, D., Rottapel, R., Saito, T., and Penninger, J. M. (2004) *J. Exp. Med.* **200,** 1167–1177
24. Sun, L., Deng, L., Ea, C. K., Xia, Z. P., and Chen, Z. J. (2004) *Mol. Cell* **14,** 289–301
25. Wang, D., Matsumoto, R., You, Y., Che, T., Lin, X. Y., Gaffen, S. L., and Lin, X. (2004) *Mol. Cell. Biol.* **24,** 164–171
26. Zhou, H., Wertz, I., O'Rourke, K., Ultsch, M., Seshagiri, S., Eby, M., Xiao, W., and Dixit, V. M. (2004) *Nature* **427,** 167–171
27. Wegener, E., Oeckinghaus, A., Papadopoulou, N., Lavitas, L., Schmidt-Supprian, M., Ferch, U., Mak, T. W., Ruland, J., Heissmeyer, V., and Krappmann, D. (2006) *Mol. Cell* **23,** 13–23
28. Niwa, H., Yamamura, K., and Miyazaki, J. (1991) *Gene (Amst.)* **108,** 193–199
29. Tanaka, J., Miwa, Y., Miyoshi, K., Ueno, A., and Inoue, H. (1999) *Biochem. Biophys. Res. Commun.* **264,** 938–943
30. Ohnuma, K., Munakata, Y., Ishii, T., Iwata, S., Kobayashi, S., Hosono, O., Kawasaki, H., Dang, N. H., and Morimoto, C. (2001) *J. Immunol.* **167,** 6745–6755
31. Tanaka, T., Duke-Cohan, J. S., Kameoka, J., Yaron, A., Lee, I., Schlossman, S. F., and Morimoto, C. (1994) *Proc. Natl. Acad. Sci. U. S. A.* **91,** 3082–3086
32. Nath, D., van der Merwe, P. A., Kelm, S., Bradfield, P., and Crocker, P. R. (1995) *J. Biol. Chem.* **270,** 26184–26191
33. Ishii, T., Ohnuma, K., Murakami, A., Takasawa, N., Kobayashi, S., Dang, N. H., Schlossman, S. F., and Morimoto, C. (2001) *Proc. Natl. Acad. Sci. U. S. A.* **98,** 12138–12143
34. Ciccimarra, F., Rosen, F. S., Schneeberger, E., and Merler, E. (1976) *J. Clin. Investig.* **57,** 1386–1390
35. Dang, N. H., Torimoto, Y., Sugita, K., Daley, J. F., Schow, P., Prado, C., Schlossman, S. F., and Morimoto, C. (1990) *J. Immunol.* **145,** 3963–3971
36. Chien, C. H., Huang, L. H., Chou, C. Y., Chen, Y. S., Han, Y. S., Chang, G. G., Liang, P. H., and Chen, X. (2004) *J. Biol. Chem.* **279,** 52338–52345
37. Rasmussen, H. B., Branner, S., Wiberg, F. C., and Wagtmann, N. (2003) *Nat. Struct. Biol.* **10,** 19–25
38. Lee, K. Y., D'Acquisto, F., Hayden, M. S., Shim, J. H., and Ghosh, S. (2005) *Science* **308,** 114–118
39. Lin, X., and Wang, D. (2004) *Semin. Immunol.* **16,** 429–435
40. Gerli, R., Muscat, C., Bertotto, A., Bistoni, O., Agea, E., Tognellini, R., Fiorucci, G., Cesarotti, M., and Bombardieri, S. (1996) *Clin. Immunol. Immunopathol.* **80,** 31–37
41. Muscat, C., Bertotto, A., Agea, E., Bistoni, O., Ercolani, R., Tognellini, R., Spinozzi, F., Cesarotti, M., and Gerli, R. (1994) *Clin. Exp. Immunol.* **98,** 252–256
42. Mizokami, A., Eguchi, K., Kawakami, A., Ida, H., Kawabe, Y., Tsukada, T., Aoyagi, T., Maeda, K., Morimoto, C., and Nagataki, S. (1996) *J. Rheumatol.* **23,** 2022–2026
43. Dong, R. P., Tachibana, K., Hegen, M., Scharpe, S., Cho, D., Schlossman, S. F., and Morimoto, C. (1998) *Mol. Immunol.* **35,** 13–21
44. Smart, E. J., Graf, G. A., McNiven, M. A., Sessa, W. C., Engelman, J. A., Scherer, P. E., Okamoto, T., and Lisanti, M. P. (1999) *Mol. Cell. Biol.* **19,** 7289–7304
45. van der Merwe, P. A., Barclay, A. N., Mason, D. W., Davies, E. A., Morgan, B. P., Tone, M., Krishnam, A. K., Ianelli, C., and Davis, S. J. (1994) *Biochemistry* **33,** 10149–10160
46. van der Merwe, P. A., Bodian, D. L., Daenke, S., Linsley, P., and Davis, S. J. (1997) *J. Exp. Med.* **185,** 393–403
47. Collins, A. V., Brodie, D. W., Gilbert, R. J., Iaboni, A., Manso-Sancho, R., Walse, B., Stuart, D. I., van der Merwe, P. A., and Davis, S. J. (2002) *Immunity* **17,** 201–210
48. Ohnuma, K., Ishii, T., Iwata, S., Hosono, O., Kawasaki, H., Uchiyama, M., Tanaka, H., Yamochi, T., Dang, N. H., and Morimoto, C. (2002) *Immunology* **107,** 325–333
49. von Bonin, A., Huhn, J., and Fleischer, B. (1998) *Immunol. Rev.* **161,** 43–53
50. Chen, C. Y., Cordeaux, Y., Hill, S. J., and King, J. R. (2003) *Bull. Math. Biol.* **65,** 933–958
51. Thome, M. (2004) *Nat. Rev. Immunol.* **4,** 348–359
52. Dimitratos, S. D., Woods, D. F., Stathakis, D. G., and Bryant, P. J. (1999) *BioEssays* **21,** 912–921
53. Marguet, D., Bernard, A. M., Vivier, I., Darmoul, D., Naquet, P., and Pierres, M. (1992) *J. Biol. Chem.* **267,** 2200–2208
54. Yan, S., Marguet, D., Dobers, J., Reutter, W., and Fan, H. (2003) *Eur. J. Immunol.* **33,** 1519–1527

INFECTION AND IMMUNITY, Jan. 2008, p. 214–220 Vol. 76, No. 1
0019-9567/08/$08.00+0 doi:10.1128/IAI.01193-07

Nonpathogenic *Escherichia coli* Strain Nissle 1917 Inhibits Signal Transduction in Intestinal Epithelial Cells[▽]

Nobuhiko Kamada,[1]† Kenichi Maeda,[2]† Nagamu Inoue,[1] Tadakazu Hisamatsu,[1] Susumu Okamoto,[1] Kyong Su Hong,[2] Takaya Yamada,[3] Noriaki Watanabe,[4] Kanji Tsuchimoto,[4] Haruhiko Ogata,[1] and Toshifumi Hibi[1]*

Division of Gastroenterology and Hepatology, Department of Internal Medicine, Keio University School of Medicine, Tokyo, Japan[1]; Research Center, Research Division, JCR Pharmaceuticals Co., Ltd., Kobe, Japan[2]; Department of Experimental Animals, Center for Integrated Research in Science, Shimane University, Izumo, Japan[3]; and Department of Internal Medicine, Kitasato Institute Hospital, Tokyo, Japan[4]

Received 30 August 2007/Returned for modification 28 September 2007/Accepted 18 October 2007

Although the probiotic *Escherichia coli* strain Nissle 1917 has been used for the treatment of inflammatory bowel diseases, the precise mechanisms of action of this strain remain unclear. In the present study, we estimated the anti-inflammatory effect of *E. coli* Nissle 1917 on inflammatory responses in vitro to determine the suppressive mechanism of Nissle 1917 on the inflammatory process. To determine the effect of *E. coli* Nissle 1917, the human colonic epithelial cell line HCT15 was incubated with or without *E. coli* Nissle 1917 or another nonpathogenic *E. coli* strain, K-12, and then tumor necrosis factor alpha (TNF-α)-induced interleukin-8 (IL-8) production from HCT15 cells was assessed. Enzyme-linked immunosorbent assays and real-time quantitative PCR showed that Nissle 1917 treatment suppressed TNF-α-induced IL-8 transcription and production. In addition, results from luciferase assays indicated that Nissle 1917 inhibited IL-8 promoter activity. On the other hand, these anti-inflammatory effects were not seen with *E. coli* K-12. In addition, heat-killed Nissle 1917 or its genomic DNA did not have this anti-inflammatory effect. Surprisingly, Nissle 1917 did not affect IL-8 transactivation pathways, such as NF-κB activation, nuclear translocation, and DNA binding, or even activation of other transcriptional factors. Furthermore, it also became evident that Nissle 1917 induced the anti-inflammatory effect without contact to epithelial cells. In conclusion, these data indicate that the nonpathogenic *E. coli* strain Nissle 1917 expresses a direct anti-inflammatory activity on human epithelial cells via a secreted factor which suppresses TNF-α-induced IL-8 transactivation through mechanisms different from NF-κB inhibition.

Inflammatory bowel disease (IBD) is a disease characterized as chronic intestinal mucosal inflammation (3). In spite of recent clinical and basic research, the etiology of IBD remains unknown (16). Recent basic research has indicated that bacterial flora play an important role in the homeostasis of gut, and a dysregulated interaction between intestinal mucosa and flora may contribute to the development and the perpetuation of intestinal inflammation (22). In some genetically engineered rodent colitis models, for example, in murine lines deficient for the T-cell receptor alpha-chain gene (12), the interleukin-10 (IL-10) gene (10), or the IL-2 gene (20) and in HLA-B27 transgenic rat lines (29), the commensal bacteria are required for the development of chronic colitis. These rodent colitis models do not develop intestinal inflammation under germ-free conditions. Some clinical evidence has also indicated the contribution of intestinal flora to the development of colitis, as antibiotics are often effective in human IBD therapy (28). Furthermore, recent linkage analysis identified a single-nucleotide polymorphism of the CARD15 gene, which is the cytosolic receptor for the bacterial cell wall component muramyl dipeptide, as associated with the risk of Crohn's disease (4, 14). Thus, the regulation of the interaction between intestinal mucosa and gut flora is considered to be a novel therapeutic strategy for IBD. Probiotics are defined as living nonpathogenic organisms that confer health benefits by improving the microbial balance (23). It has been reported that probiotics have demonstrated efficacy in the treatment of human IBD (23). Nonpathogenic *Escherichia coli* strain Nissle 1917 is the active component of the microbial drug Mutaflor (Ardeypharm, Germany). This strain is used in several European countries as a probiotic drug for the treatment of IBD. Recent clinical trials have demonstrated the efficacy of Nissle 1917 for the treatment ulcerative colitis (8, 9, 18). Nissle 1917 had equivalent efficacy to mesalazine, which is commonly used for treating IBD, in the maintenance of remission of ulcerative colitis. Although several mechanisms of action have been suggested to explain the protective and anti-inflammatory effect of probiotics, the precise mechanism remains unclear. In this study, we investigated the anti-inflammatory effect of *E. coli* Nissle 1917 on proinflammatory cytokine production from intestinal epithelial cells (IECs).

* Corresponding author. Mailing address: Division of Gastroenterology and Hepatology, Department of Internal Medicine, Keio University School of Medicine, 35 Shinano-machi, Shinjuku-ku, Tokyo 160-8582, Japan. Phone and fax: 81 3 3357 6156. E-mail: thibi@sc.itc.keio.ac.jp.

† N.K. and K.M. contributed equally to this work.

▽ Published ahead of print on 29 October 2007.

MATERIALS AND METHODS

Cell culture. HCT15 cells were cultured in Dulbecco's modified Eagle's medium (DMEM) (Sigma, St. Louis, MO) supplemented with 10% heat-inactivated

fetal bovine serum (Biosource International, CA). The cells were inoculated into six-well plates (1.0×10^6 cells/well) and then incubated overnight at 37°C.

Preparation of bacteria. The *E. coli* strain Nissle 1917 (Mutaflor; DMS 6601, serotype O6:K5:H1) was kindly provided by Ardeypharm GmbH (Herdecke, Germany). Nissle 1917 and the nonpathogenic *E. coli* K-12 DH10B strain were used in this study. Bacteria were incubated in Luria-Bertani medium at 37°C in a shaker to reach mid-log phase with the density determined as 0.5 to 0.7 at A_{600}. Bacteria were collected by centrifugation, washed twice with phosphate-buffered saline (PBS), and resuspended in DMEM at up to 1.0×10^5 CFU/ml. Heat-killed bacteria were prepared by resuspending viable bacteria in PBS, followed by incubation for 30 min at 60°C. Killed bacteria were then washed with PBS and resuspended in PBS. Genomic DNA was isolated from Nissle 1917 using a Genomic DNA isolation kit (Qiagen Inc., Valencia, CA).

Treatment for *E. coli* on human IECs. The *E. coli* prepared at 1.0×10^5 CFU/ml were applied to HCT15 cells and coincubated for various lengths of time. After *E. coli* preincubation, HCT15 cells were stimulated with 20 ng/ml of tumor necrosis factor alpha (TNF-α) for 30 min without removing the bacteria. Cells were washed once with cold PBS and scraped with a cell scraper. Cells were collected and washed twice with ice-cold PBS.

ELISA) for IL-8. Collected cells were suspended in lysis buffer (0.5% NP-40, 10 mM Tris-HCl [pH 7.4], 150 mM NaCl, 1 mM EDTA, 1 mM phenylmethylsulfonyl fluoride, 10 μg/ml aprotinin, 10 μg/ml leupeptin) and left to stand on ice for 25 min. The cell lysate was centrifuged at 15,000 rpm for 5 min, and then insoluble debris was removed. The interleukin-8 (IL-8) concentration of the HCT15 cell extraction was measured by an enzyme-linked immunosorbent assay (ELISA) kit (Biosource).

Analysis of IL-8 expression by RT-PCR. HCT15 cells were incubated with live Nissle 1917 (1.0×10^5 CFU/ml), heat-killed Nissle 1917 (1.0×10^8 CFU/ml), or its genomic DNA (10 μg/ml) for 4 h and then stimulated by TNF-α. Cells were harvested after a 30-min stimulation, and total RNA was isolated using an RNeasy mini kit (Qiagen). In this process, RNA was treated with RNase-free DNase I (Qiagen) to prevent carryover of genomic DNA. The cDNA was synthesized from 2 μg of total RNA with Omniscript reverse transcriptase (Qiagen). For quantitative reverse transcription-PCR (RT-PCR), equivalent amounts of cDNAs (2 μl) and 0.5 μM concentrations of the forward and the reverse primers were used with a DyNAmo Sybr Green quantitative PCR (qPCR) kit (MJ Research, Waltham, MA). The PCRs were carried out in a thermocycler DNA Engine, Opticon2 (MJ Research). Cycling conditions for PCR amplification were 95°C for 10 min and 40 cycles of 95°C for 10 s and 58°C for 50 s. Human specific primers for IL-8 were 5′-TCTGCAGCTCTGTGTGAAGGTGCAGT T-3′ (forward) and 5′-AACCCTCTGCACCCAGTTTTCCT-3′ (reverse). β-Actin primers were 5′-CTACGTCGCCCTGGACTTCGAGC-3′ (forward) and 5′-GATGGAGCCGCCGATCCACACG-3′ (reverse).

Construction of IL-8 luciferase reporter constructs. The 5′ deletion constructs of the human IL-8 promoter corresponding to sequences from −1481 (pNAF), −130 (pN130), −112 (pN112), and −78 (pN78) to +44 bp and a promoterless plasmid (pLuc0) were kindly provided by S. Abe (Yamagata University, Japan). Site-directed mutagenesis of the IL-8 promoter was performed using a QuickChange site-directed mutagenesis kit (Stratagene). The construct containing the −130-bp sequence upstream from the transcription start site of the IL-8 gene (pN130) was used as a template plasmid. The primers used for point mutations for the activator protein 1 (AP-1) site (at −126 to −120, TGACTCA to TATC TCA; mutation is underlined) were 5′-GTGTGATATCTCAGGTTTGCCCTG AGGG-3′ (forward) and 5′-CCCTCAGGGCAAACCTGAGATATCACAC-3′ (reverse). For C/EBPβ (point mutations at −94 to −81, CAGTTGCAAATCGT to AGCTTGCAAATCGT), the primers were 5′-GGATGGGCCATAGCTTG CAAATCGTGG-3′ (forward) and 5′-CCACGATTTGCAAGCTATGGCCCA TCC-3′ (reverse). For NF-κB (point mutations at −80 to −71, GGAATTTCCT to TAACTTTCCT), the primers were 5′-GTTGCAAATCGTTAACTTTCCTC TGACATAATG3′ (forward) and 5′-CATTATGTCAGAGGAAAGTTAACG ATTTGCAAC-3′ (reverse). These plasmid constructs were confirmed by sequencing.

DNA transfection and luciferase reporter assay. A total of 1×10^6 HCT15 cells/well were seeded on six-well plates. After 24 h, the cells were transiently transfected with the indicated reporter plasmid (1 μg/well) with the *Renilla* luciferase expression plasmid pRL-TK (0.1 μg/ml) (Promega), using FuGENE 6 transfection reagent (Roche). After incubation of 24 h, cells were washed twice with PBS and cultured for 4 h in serum and antibiotic-free Hank's balanced buffered salt containing calcium chloride with or without Nissle 1917 (1.0×10^7 CFU/ml). Cells were then stimulated by TNF-α (20 ng/ml) for 30 min. The luciferase activity of total cell lysates was measured using a dual luciferase reporter assay system (Promega). The *Renilla* luciferase reporter gene pRL-TK was used as an internal control.

Western blot analysis. HCT15 cells were grown in six-well plates. The cells were pretreated with 1.0×10^5 CFU/ml Nissle 1917 for 4 h and then stimulated with 20 ng/ml of TNF-α. Total cell lysates and nuclear protein from HCT15 cells were obtained using mammalian protein extraction reagent and a nuclear and cytosol protein extraction kit (Pierce). Each protein was fractionated by sodium dodecyl sulfate-polyacrylamide gel electrophoresis and transferred onto polyvinylidene difluoride membranes (Millipore). Membranes were blocked with 5% milk and incubated overnight with anti-p65 polyclonal antibody (Santa Cruz), anti-IκBα polyclonal antibody (Santa Cruz), or anti-β-actin polyclonal antibody (Sigma) at 4°C, followed by incubation at room temperature for 1 h with horseradish peroxidase-linked anti-rabbit antibody (Cell Signaling). Staining was detected using ECL Western blotting detection reagent (Amersham Biosciences).

Nuclear protein extraction and electrophoretic mobility shift assay (EMSA). Nuclear extracts were prepared from HCT15 cells using a nuclear and cytosol protein extraction kit (Pierce). Both double-stranded oligonucleotide probes corresponding to the wild-type NF-κB binding site (5′-AGTTGAGGGGACTT TCCCAGGC-3′ and 3′-TCAACTCCCCTGAAAGGGTCCG-5′ [Promega]) and the mutated NF-κB binding site (5′-AGTTGAGGCGACTTTCCCAGG C-3′ and 3′-TCAACTCCGCTGAAAGGGTCCG-5′; mutations are underlined [Santa Cruz]) were used as probes or cold competitors to analyze the interaction between NF-κB and DNA. The probes were labeled with [γ-^{32}P]ATP (3,000 Ci/mmol at 10 mCi/ml) (Amersham Biosciences) using T4 polynucleotide kinase (Promega) and purified by MicroSpin G-25 columns (Amersham Biosciences). The binding reaction was performed using a gel shift assay system (Promega) and 20 μg of nuclear extract. For the competition assay, a 100-fold excess of unlabeled oligonucleotide was added to the reaction mixture. Samples were electrophoresed by a 4% nondenaturing acrylamide gel in 0.5× Tris-borate-EDTA buffer at 150 V for 1.5 h. The gel was placed on a filter paper and dried with a Gel Dryer (Bio-Rad) for 1 h. Then, the gel was exposed to a phosphorimaging plate overnight and analyzed by BAS 2000 systems.

ChIP assay. The HCT15 cells were cross-linked by 1% formaldehyde for 15 min at 37°C. Cross-linking was stopped by the addition of 0.125 M glycine, and cells were incubated for 10 min at 4°C and then washed twice with ice-cold PBS. Following cross-linking, the cells were collected and resuspended in sodium dodecyl sulfate lysis buffer (Upstate) containing protease inhibitors (1 mM phenylmethylsulfonyl fluoride, 1 μg/ml aprotinin, and 1 μg/ml leupeptin), and the chromatin was cleaved into 500- to 1,000-bp fragments by sonication. Samples were then diluted with chromatin immunoprecipitation (ChIP) dilute buffer and incubated overnight with 3 μg of specific antibodies for p65 (Upstate) or RNA polymerase II (Santa Cruz), followed by incubation with protein A-agarose saturated with bovine serum albumin and salmon sperm DNA. Agarose-bound immune complexes were collected, washed, and eluted. The protein-DNA cross-links were incubated overnight at 65°C to reverse cross-links. After proteinase K digestion, DNA was purified using a PCR purification kit (Qiagen). Purified immunoprecipitated chromatin and input samples were analyzed by real-time qPCR using a DyNAmo Sybr Green qPCR kit and the thermocycler DNA Engine Opticon2 (MJ Research). Primer pairs for monitoring the IL-8 promoter region were 5′GGGCCATCAGTTGCAAATC-3′ (forward) and 5′-TTCCTTCCGGTGGTTTCTTC-3′ (reverse). Cycling conditions for PCR amplification were 95°C for 10 min and 40 cycles of 95°C for 10 s and 58°C for 50 s.

Analysis of the suppressive effect of Nissle 1917 secreted factor. HCT15 cells were cultured in the lower well of the Transwell filter membrane system (0.4-μm pore size; Costar). *E. coli* Nissle 1917 or K-12 DH10B prepared at 1.0×10^5 CFU/ml was applied to the upper well and coincubated for 4 h. After preincubation, cells were stimulated with 20 ng/ml of TNF-α for 30 min. In a separate test, Nissle 1917 or K-12 DH10B (1.0×10^5 CFU/ml) alone was incubated in DMEM for 4 h, and then supernatants were separated by passage through 0.22-μm-pore-size filters. Filtered culture supernatants were then applied to the HCT15 cells and incubated for 30 min. After incubation, cells were stimulated with 20 ng/ml of TNF-α for 30 min. For both culture methods, after stimulation with TNF-α, cells were washed once with cold PBS and scraped with a cell scraper. Cells were then collected and washed twice with ice-cold PBS. Cellular proteins were extracted by the protein extraction method, described above, and IL-8 concentrations were measured by ELISA.

Statistical analysis. Statistical analysis was performed using GraphPad Prism software, version 4.0 (San Diego, CA). Differences at a P value of <0.05 were considered to be significant. All data are expressed as means ± standard error of the mean (SEM).

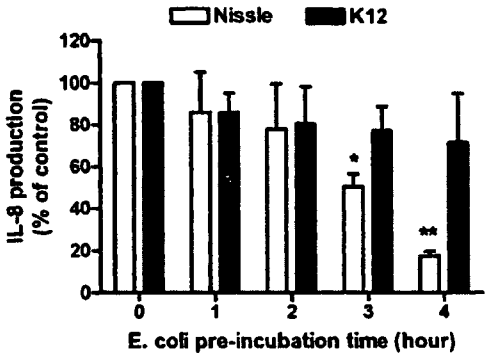

FIG. 1. *E. coli* Nissle 1917 suppresses TNF-α-induced IL-8 production. HCT15 cells were pretreated for various lengths of time with 1 × 10^5 CFU/ml nonpathogenic *E. coli* strain Nissle 1917 or K-12 DH10B and were then stimulated with 20 ng/ml TNF-α for 30 min. After stimulation, intracellular proteins were extracted, and IL-8 protein amounts were determined by ELISA. Data are expressed as the percentage of IL-8 production in HCT15 cells stimulated with TNF-α without Nissle 1917 treatment (defined as 100%) and are given as means ± SEM of three to four experiments. Significance was determined by comparison with the values of TNF-α-induced IL-8 in the *E. coli* untreated group (Dunnett's test). *, $P < 0.05$; **, $P < 0.01$.

RESULTS

***E. coli* Nissle 1917 inhibited TNF-α-induced IL-8 production by IECs.** To determine the effect of Nissle 1917, human IEC line HCT15 cells were untreated or pretreated with *E. coli* Nissle 1917 and another nonpathogenic *E. coli* strain, K-12 DH10B (1 × 10^5 CFU/ml), for 1 to 4 h, followed by stimulation with TNF-α (20 ng/ml) for 30 min. After stimulation, the intracellular protein levels of the proinflammatory chemokine IL-8 were assayed by ELISA. The basal production of IL-8 was not affected by *E. coli* Nissle 1917 and K-12; however, TNF-α-induced IL-8 production was significantly inhibited by a 3- to 4-h pretreatment with Nissle 1917 but not by K-12 (Fig. 1). Another enteric *E. coli* strain, ATCC 25922, did not show the inhibitory effect on TNF-α-induced IL-8 production, similar to K-12 (data not shown). These results suggest that only the probiotic strain Nissle 1917 has an anti-inflammatory effect among the nonpathogenic *E. coli* strains. Next, we examined the effect of Nissle 1917 on IL-8 mRNA expression after TNF-α stimulation using real-time qPCR. Consistent with the result of protein production, TNF-α-induced IL-8 mRNA transcription was also suppressed by pretreatment with *E. coli* Nissle 1917 (Fig. 2A) but not by *E. coli* K-12 (data not shown). Moreover, the proinflammatory chemokine methyl-accepting chemotaxis protein 1, which was strongly induced by TNF-α, was also suppressed by Nissle 1917 (data not shown). Because recent studies have reported that genomic DNA itself has anti-inflammatory effects in vitro and in vivo (5, 7, 17), we investigated the effect of genomic DNA from Nissle 1917 and heat-killed Nissle 1917 on IL-8 production from TNF-α-treated HCT15 cells. As shown in Fig. 2B, heat-killed Nissle 1917 and its genomic DNA did not show such an anti-inflammatory effect. These results indicated that only the live *E. coli* Nissle 1917, and not heat-killed and genomic DNA alone, can inhibit TNF-α-induced IL-8 production, even in the transcriptional process.

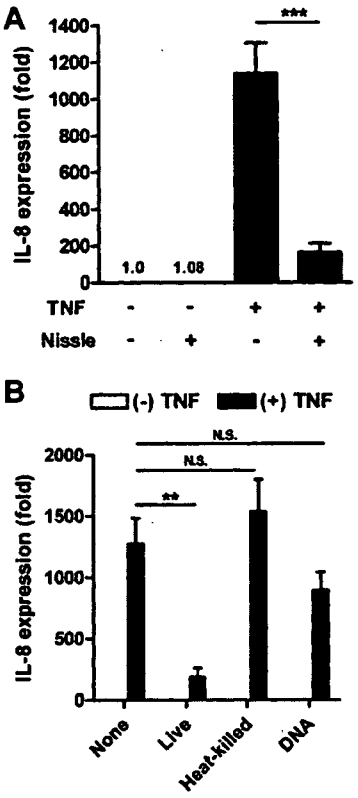

FIG. 2. *E. coli* Nissle 1917 suppresses TNF-α-triggered transcription of IL-8 via its viable form. (A) HCT15 cells were pretreated with Nissle 1917 (1 × 10^5 CFU/ml) for 4 h and then stimulated with 20 ng/ml TNF-α. After stimulation for 30 min, IL-8 mRNA expression was analyzed by real-time RT-PCR. (B) HCT15 cells were pretreated with living Nissle 1917 bacteria (1 × 10^5 CFU/ml), heat-killed Nissle 1917 (1 × 10^8 CFU/ml), or its genomic DNA (10 μg/ml) for 4 h and then stimulated by 20 ng/ml TNF-α for 30 min. IL-8 mRNA expression was analyzed by real-time RT-PCR. Data are shown as relative expression against β-actin mRNA and given as means ± SEM of five independent experiments. Significance was determined by comparison with the values of TNF-α-induced IL-8 in the *E. coli* untreated group (Sheffe's test). **, $P < 0.01$; ***, $P < 0.001$.

***E. coli* Nissle 1917 suppresses the promoter activity of human IL-8.** To identify the transcriptional regulation of IL-8 by Nissle 1917, a series of luciferase reporter plasmids of the IL-8 promoter were used. As shown in Fig. 3A, luciferase activity in HCT15 cells transfected with a vector containing the entire 1,481-bp upstream DNA fragment (pNAF1481) was higher than that obtained with the empty pLuc0 vector by TNF-α stimulation. Promoter activity was significantly decreased in pN78 compared with pN112. This result indicated that the sequence upstream of −78 is required for TNF-α-induced IL-8 promoter activity. Consistent with the results of real-time PCR and ELISA, Nissle 1917 pretreatment suppressed the TNF-α-induced transactivation of IL-8 promoter activity in both pN130 and the deletion mutant of the AP-1 binding sequence, pN112. This result suggests that AP-1 is not the crucial target for the suppressive effect of Nissle 1917 on TNF-α-induced IL-8 transactivation. In addition, the nonpathogenic *E. coli* strain K-12 did not inhibit IL-8 promoter activity in either ELISA or RT-PCR analysis (data not shown). To identify the

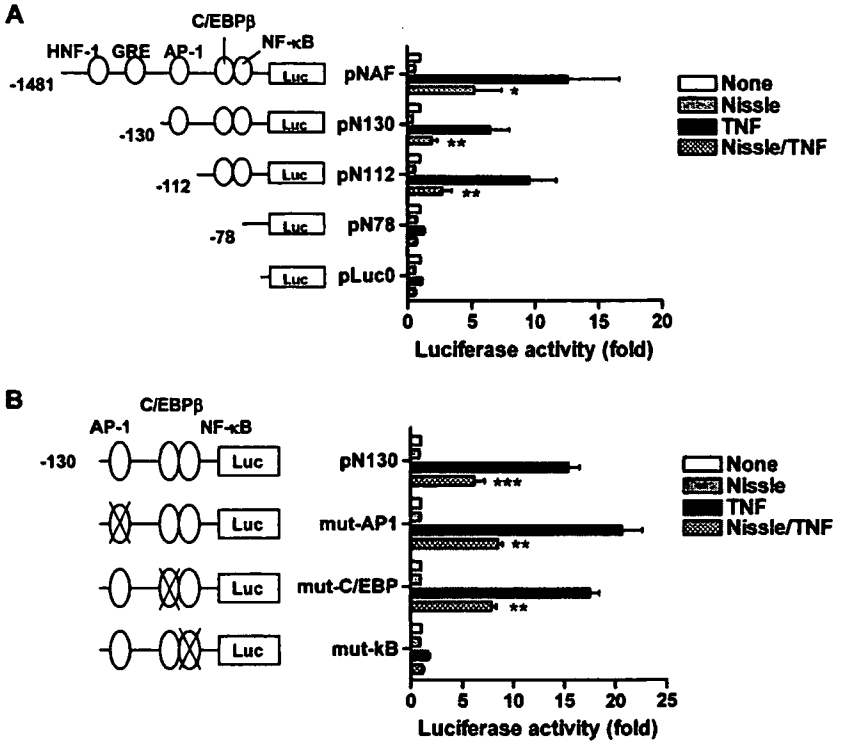

FIG. 3. Nissle 1917 inhibits IL-8 promoter activity. (A) HCT15 cells were transfected with 5′ deletions of the IL-8 promoter-driven luciferase. Each sample contained *Renilla* luciferase vector DNA (pRL-TK) for normalization of transfection efficiency. Twenty-four hours after transfection, cells were treated with Nissle 1917 bacteria (1.0×10^7 CFU/ml) for 4 h in serum-free Hank's balanced salt solution and then stimulated with TNF-α for 30 min. Cells were lysed and assayed for luciferase activity. (B) The proximal human IL-8 promoter region (position −130) was used for mutation assays. Mutant (mut) vectors of NF-κB, C/EBPβ, or AP-1 binding sites were transfected into HCT15 cells and then treated with Nissle 1917 and TNF-α, as described above. Cells were lysed and assayed for luciferase activity. The results are presented as the relative increase in activation (*n*-fold) of control cells and are given as means ± SEM of four to six independent experiments. Significance was determined by comparison with the values of TNF-α-induced IL-8 in the *E. coli* untreated group (paired Student's *t* test). *, $P < 0.05$; **, $P < 0.01$; ***, $P < 0.001$. GRE, glucocorticoid response element.

responsible element of the IL-8 promoter sequence in the Nissle 1917-mediated inhibition, mutated constructs of each transcription factor binding sequence were generated (Fig. 3B). As a result of the deletion study, a mutated construct in the AP-1 binding site showed increased luciferase activity as a result of TNF-α stimulation and the inhibitory effects of Nissle 1917. Moreover, the construct with a mutation of the C/EBPβ (CCAAT/enhancer-binding protein β) binding site also had a normal response to TNF-α stimulation and decreased luciferase activity with Nissle 1917 pretreatment. These results suggest that AP-1 and C/EBPβ were not responsible for the suppressive effect of Nissle 1917. However, up-regulation of luciferase activity by TNF-α stimulation was completely suppressed by mutation of the NF-κB binding site, as indicated by the results of the deletion study.

To investigate whether Nissle 1917 can inhibit NF-κB activation, which is considered the element responsible for the augmentation of IL-8 transcription by TNF-α, we next analyzed the activation of NF-κB by Western blot analysis. In the normal state, NF-κB exists in the cytoplasm as a nonactivated complex consisting of three subunits: a transactivating subunit p65 (also called RelA), p50, and an inhibitory subunit, IκBα. With exposure to an inflammatory stimulus such as TNF-α, the inhibitory subunit IκBα is phosphorylated and degraded; then the transactivating subunit p65-p50 heterodimer is translocated into the nucleus. As shown in Fig. 4A and B, IκBα degradation and nuclear translocation of the p65 subunit were observed after TNF-α stimulation. However, treatment with Nissle 1917 did not suppress these processes. These data indicate that Nissle 1917 does not affect the nuclear translocation of p65. To determine whether Nissle 1917 prevented the DNA binding process of transcriptional factors, we carried out EMSAs. As shown in Fig. 4C, TNF-α stimulation increased DNA binding of NF-κB, but this was not inhibited by Nissle 1917 treatment (lanes 3 and 4). Another transcriptional factor, C/EBPβ, did not prevent DNA binding with Nissle 1917 treatment (data not shown). Since EMSAs assessed the binding of NF-κB consensus motifs in vitro, p65 recruitment to the endogenous IL-8 promoter in intact cells was tested by ChIP assay. Stimulation of TNF-α caused extensive recruitment of the p65 NF-κB subunit and transcriptional cofactor CBP to the IL-8 promoter, and this was not blocked by Nissle 1917 treatment (Fig. 4D). Thus, the suppressive effect of Nissle 1917 on the transcription of TNF-α-induced IL-8 is independent of the NF-κB activation process.

Nissle 1917 secreted factor suppressed TNF-a induced IL-8 production. To determine the anti-inflammatory effect of Nissle 1917 secreted factors, we used the Transwell system

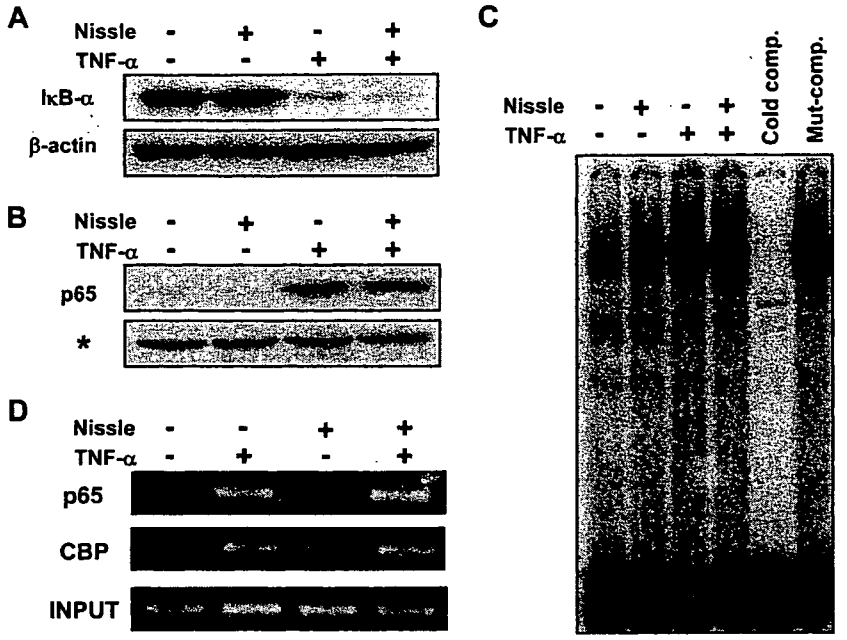

FIG. 4. Nissle 1917 does not affect NF-κB transactivation pathways. (A) HCT15 cells were pretreated with Nissle 1917 bacteria (1×10^5 CFU/ml) for 4 h and then stimulated with 20 ng/ml TNF-α. After stimulation for 30 min, whole cellular proteins were extracted and used for Western blotting of IκBα and β-actin. (B) HCT15 cells were treated with Nissle 1917 and TNF-α as before, and then nuclear proteins were extracted. Extracted nuclear proteins were used for NF-κB p65 Western blotting. A nonspecific protein recognized by the antibody was used as loading control (asterisk). Data are representative of one of three independent experiments. (C) HCT15 cells were pretreated with Nissle 1917 bacteria (1×10^5 CFU/ml) for 4 h and then stimulated with 20 ng/ml TNF-α. After stimulation for 30 min, nuclear proteins were extracted. EMSAs were performed with a ^{32}P-labeled probe containing the NF-κB binding site and nuclear extracts from TNF-α-stimulated HCT15 cells with or without Nissle 1917 pretreatment. Data are representative of one of three independent experiments. (D) HCT15 cells were pretreated with Nissle 1917 bacteria (1×10^5 CFU/ml) for 4 h and then stimulated with 20 ng/ml TNF-α for 30 min. ChIP assays were performed with the indicated antibodies. The detection of the immunoprecipitated human IL-8 promoter was analyzed by PCR with promoter-specific primers. Data are representative of one of three independent experiments. Mut, mutant; comp, competitor.

(Fig. 5A) and *E. coli* culture supernatant (Fig. 5B) in tandem with control strain K-12 for the IL-8 prevention assay. Interestingly, Nissle 1917 inhibited TNF-α-induced IL-8 production but not through contact with the cells. These results suggest that a currently unknown Nissle 1917 secreted factor in the culture supernatant suppressed the TNF-α-triggered inflammatory processes.

DISCUSSION

IECs play a role as a barrier both functionally and structurally. IECs separate the host's internal milieu from the external environment. In addition to the barrier function, it has become evident recently that IECs play an important role in maintaining homeostasis. IECs produce antimicrobial peptides, such as defensins, and protect the host from attachment of luminal bacteria (21, 30). Moreover, in addition to a direct bactericidal role, IEC-derived factors can promote an anti-inflammatory type of dendritic cells and macrophages differentiation to induce mucosal tolerances against luminal bacteria (19, 26). Furthermore, IECs can produce several chemokines and proinflammatory cytokines to induce the migration of granulocytes, lymphocytes, and dendritic cells, resulting in the induction of host immunity (1). Previous studies have demonstrated that IECs produce IL-8 in response to several pathogenic bacteria (6). Thus, IECs function as a defensive frontline of host mucosal immunity. Although the therapeutic mechanism of action

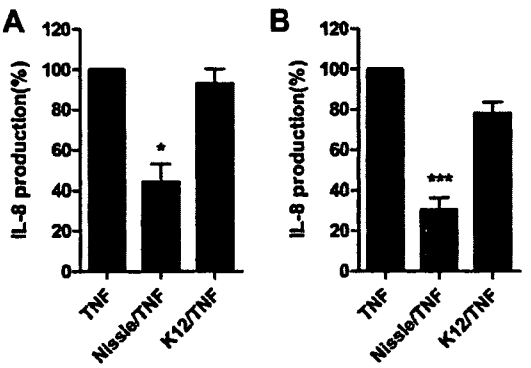

FIG. 5. Nissle 1917 inhibited TNF-α-induced IL-8 production without adherence of bacteria to the epithelial cells. (A) HCT15 cells were cultured in the lower well of a Transwell filter membrane system (0.4-μm pore size). *E. coli* Nissle 1917 or K-12 DH10B prepared at 1.0×10^5 CFU/ml was applied to the upper well and coincubated for 4 h. After preincubation, cells were stimulated with 20 ng/ml of TNF-α for 30 min. (B) *E. coli* Nissle 1917 or K-12 DH10B (1.0×10^5 CFU/ml) alone was incubated in DMEM for 4 h, and then supernatants were separated by passage through a 0.22-μm-pore-size filter. Filtered culture supernatants were then applied to the HCT15 cells and incubated for 30 min. After incubation, cells were stimulated with 20 ng/ml of TNF-α for 30 min. After stimulation, intracellular proteins were extracted, and IL-8 protein amounts were determined by ELISA. Data are expressed as the percentage of IL-8 production in *E. coli* untreated controls (defined as 100%). Data are given as means ± SEM of the at least three experiments. *, $P < 0.05$; ***, $P < 0.001$ (Dunnett's test).

of probiotics in IBD remains unclear, it was previously reported that some nonpathogenic resident bacteria and probiotic bacteria strains suppress IL-8 production from IECs. For example, nonpathogenic *Salmonella enterica* serovar Typhimurium (13), *Lactobacillus reuteri* (11), or the probiotic VSL#3 (5) prevented TNF-α-induced IL-8 production. These suppressive functions of nonpathogenic resident bacteria and probiotic strains may contribute to maintaining intestinal homeostasis or show therapeutic effects as a probiotics. Consistent with studies of other probiotic bacteria, we found a suppressive effect of nonpathogenic *E. coli* Nissle 1917 on TNF-α-induced IL-8 production. This function is one of the therapeutic mechanisms of Nissle 1917 on IBD. There have been some reports on the inhibitory mechanisms of the signal transduction pathway by probiotic bacteria: a nonpathogenic *Salmonella* species was found to inhibit IκB ubiquitination and the subsequent NF-κB activation (13); *L. reuteri* inhibited IκB degradation (11); VSL#3 suppressed the NF-κB activation pathway through proteosome inhibition (15); and genomic DNA from VSL#3 inhibited the phosphorylation of p38 mitogen-activated protein kinase (5). In our present study, Nissle 1917 did not inhibit any of the signal transduction pathways described above, although mRNA transcription of IL-8 was suppressed. In fact, IκB degradation, NF-κB p65 nuclear translocation, and DNA binding were not dramatically altered even after Nissle 1917 treatment. These results indicated that Nissle 1917 does not suppress the NF-κB activation pathway, in contrast to *L. reuteri*. Moreover, our study demonstrated that Nissle 1917 does not affect another signal transduction pathway for IL-8 expression, namely, activation of C/EBPβ and phosphorylation of p38 mitogen-activated protein kinase (data not shown). Therefore, how does Nissle 1917 prevent IL-8 transcription if not through the inhibition of NF-κB or activation of other transcriptional factors? There is a possibility that Nissle 1917 may suppress the post-DNA binding process of transcriptional factors, prevent activation of basic transcriptional factors or RNA polymerase, or suppress chromatin remodeling processes, such as phosphorylation or acetylation of histones.

What is the active component of probiotic bacteria that is responsible for their anti-inflammatory function? Ma et al. demonstrated that *L. reuteri* inhibited TNF-α-induced IL-8 expression only through the viable form (11), and Petrof et al. reported that the VSL#3 secreted factor prevented NF-κB activation (15). In contrast, it was also demonstrated by Jijon et al. and Rachmilewitz et al. that VSL#3 genomic DNA had an anti-inflammatory function in vitro and in vivo (5, 17). We have already demonstrated that Nissle 1917 heat-killed antigen and its genomic DNA can prevent murine colitis (7). However, in our present data, heat-killed Nissle 1917 or its DNA could not suppress the TNF-α-induced IL-8 expression from IECs. This suppressive effect on the production of IL-8 from IECs was displayed only by live Nissle 1917 bacteria. Recently, the therapeutic mechanisms of Nissle 1917 have been proposed based on results from in vitro experiments. For example, Nissle 1917 increased the expression of antibacterial peptides, human β-defensins, by epithelial cell lines through the NF-κB and AP-1 pathways (24, 31); Nissle 1917 modulated T-cell cycling and expansion via Toll-like receptor 2 (TLR2) signaling (27). In addition, an anti-inflammatory effect of Nissle 1917 was reported by some investigators using in vivo experiments in several models of murine experimental colitis. We along with other groups have reported that Nissle 1917 treatment prevented both acute and chronic colitis via suppression of the production of proinflammatory cytokines by mesenteric lymph nodes or lamina propria mononuclear cells (7, 25). Moreover, Grabig et al. reported that Nissle 1917 ameliorated acute dextran sodium sulfate-induced colitis via a TLR2- and TLR4-dependent pathway (2). In the present study, we have demonstrated the first direct evidence of the anti-inflammatory effect of Nissle 1917. The findings presented here could support the anti-inflammatory effect of Nissle 1917 in murine and human intestinal inflammation.

In conclusion, we have provided evidence that the probiotic *E. coli* strain Nissle 1917 as well as other probiotic strains suppresses TNF-α-induced IL-8 secretion from IECs. Moreover, the mechanism by which Nissle 1917 suppresses IL-8 might be independent of the inhibition of the NF-κB signaling pathway. Thus, our findings may provide new insight into the mechanisms of action of the probiotic strain Nissle 1917 in IBD.

ACKNOWLEDGMENTS

We thank A. Abe for helpful advice and S. Abe for providing us with IL-8 promoter products.

This work was supported in part by grants from JCR Pharmaceuticals Co., Ltd. (Kobe, Japan).

REFERENCES

1. **Dahan, S., F. Roth-Walter, P. Arnaboldi, S. Agarwal, and L. Mayer.** 2007. Epithelia: lymphocyte interactions in the gut. Immunol. Rev. **215**:243–253.
2. **Grabig, A., D. Paclik, C. Guzy, A. Dankof, D. C. Baumgart, J. Erckenbrecht, B. Raupach, U. Sonnenborn, J. Eckert, R. R. Schumann, B. Wiedenmann, A. U. Dignass, and A. Sturm.** 2006. *Escherichia coli* strain Nissle 1917 ameliorates experimental colitis via Toll-like receptor 2- and Toll-like receptor 4-dependent pathways. Infect. Immun. **74**:4075–4082.
3. **Hibi, T., and H. Ogata.** 2006. Novel pathophysiological concepts of inflammatory bowel disease. J. Gastroenterol. **41**:10–16.
4. **Hugot, J. P., M. Chamaillard, H. Zouali, S. Lesage, J. P. Cezard, J. Belaiche, S. Almer, C. Tysk, C. A. O'Morain, M. Gassull, V. Binder, Y. Finkel, A. Cortot, R. Modigliani, P. Laurent-Puig, C. Gower-Rousseau, J. Macry, J. F. Colombel, M. Sahbatou, and G. Thomas.** 2001. Association of NOD2 leucine-rich repeat variants with susceptibility to Crohn's disease. Nature **411**:599–603.
5. **Jijon, H., J. Backer, H. Diaz, H. Yeung, D. Thiel, C. McKaigney, C. De Simone, and K. Madsen.** 2004. DNA from probiotic bacteria modulates murine and human epithelial and immune function. Gastroenterology **126**: 1358–1373.
6. **Jung, H. C., L. Eckmann, S. K. Yang, A. Panja, J. Fierer, E. Morzycka-Wroblewska, and M. F. Kagnoff.** 1995. A distinct array of proinflammatory cytokines is expressed in human colon epithelial cells in response to bacterial invasion. J. Clin. Investig. **95**:55–65.
7. **Kamada, N., N. Inoue, T. Hisamatsu, S. Okamoto, K. Matsuoka, T. Sato, H. Chinen, K. S. Hong, T. Yamada, Y. Suzuki, T. Suzuki, N. Watanabe, K. Tsuchimoto, and T. Hibi.** 2005. Nonpathogenic *Escherichia coli* strain Nissle 1917 prevents murine acute and chronic colitis. Inflamm. Bowel Dis. **11**:455–463.
8. **Kruis, W., P. Fric, J. Pokrotnieks, M. Lukas, B. Fixa, M. Kascak, M. A. Kamm, J. Weismueller, C. Beglinger, M. Stolte, C. Wolff, and J. Schulze.** 2004. Maintaining remission of ulcerative colitis with the probiotic *Escherichia coli* Nissle 1917 is as effective as with standard mesalazine. Gut **53**: 1617–1623.
9. **Kruis, W., E. Schutz, P. Fric, B. Fixa, G. Judmaier, and M. Stolte.** 1997. Double-blind comparison of an oral *Escherichia coli* preparation and mesalazine in maintaining remission of ulcerative colitis. Aliment Pharmacol. Ther. **11**:853–858.
10. **Kühn, R., J. Lohler, D. Rennick, K. Rajewsky, and W. Muller.** 1993. Interleukin-10-deficient mice develop chronic enterocolitis. Cell **75**:263–274.
11. **Ma, D., P. Forsythe, and J. Bienenstock.** 2004. Live *Lactobacillus reuteri* is essential for the inhibitory effect on tumor necrosis factor alpha-induced interleukin-8 expression. Infect. Immun. **72**:5308–5314.
12. **Mombaerts, P., E. Mizoguchi, M. J. Grusby, L. H. Glimcher, A. K. Bhan, and**

S. Tonegawa. 1993. Spontaneous development of inflammatory bowel disease in T cell receptor mutant mice. Cell 75:274–282.
13. Neish, A. S., A. T. Gewirtz, H. Zeng, A. N. Young, M. E. Hobert, V. Karmali, A. S. Rao, and J. L. Madara. 2000. Prokaryotic regulation of epithelial responses by inhibition of IκB-α ubiquitination. Science 289:1560–1563.
14. Ogura, Y., D. K. Bonen, N. Inohara, D. L. Nicolae, F. F. Chen, R. Ramos, H. Britton, T. Moran, R. Karaliuskas, R. H. Duerr, J. P. Achkar, S. R. Brant, T. M. Bayless, B. S. Kirschner, S. B. Hanauer, G. Nunez, and J. H. Cho. 2001. A frameshift mutation in NOD2 associated with susceptibility to Crohn's disease. Nature 411:603–606.
15. Petrof, E. O., K. Kojima, M. J. Ropeleski, M. W. Musch, Y. Tao, C. De Simone, and E. B. Chang. 2004. Probiotics inhibit nuclear factor-κB and induce heat shock proteins in colonic epithelial cells through proteasome inhibition. Gastroenterology 127:1474–1487.
16. Podolsky, D. K. 2002. Inflammatory bowel disease. N. Engl. J. Med. 347: 417–429.
17. Rachmilewitz, D., K. Katakura, F. Karmeli, T. Hayashi, C. Reinus, B. Rudensky, S. Akira, K. Takeda, J. Lee, K. Takabayashi, and E. Raz. 2004. Toll-like receptor 9 signaling mediates the anti-inflammatory effects of probiotics in murine experimental colitis. Gastroenterology 126:520–528.
18. Rembacken, B. J., A. M. Snelling, P. M. Hawkey, D. M. Chalmers, and A. T. Axon. 1999. Non-pathogenic *Escherichia coli* versus mesalazine for the treatment of ulcerative colitis: a randomised trial. Lancet 354:635–639.
19. Rimoldi, M., M. Chieppa, V. Salucci, F. Avogadri, A. Sonzogni, G. M. Sampietro, A. Nespoli, G. Viale, P. Allavena, and M. Rescigno. 2005. Intestinal immune homeostasis is regulated by the crosstalk between epithelial cells and dendritic cells. Nat. Immunol. 6:507–514.
20. Sadlack, B., H. Merz, H. Schorle, A. Schimpl, A. C. Feller, and I. Horak. 1993. Ulcerative colitis-like disease in mice with a disrupted interleukin-2 gene. Cell 75:253–261.
21. Salzman, N. H., M. A. Underwood, and C. L. Bevins. 2007. Paneth cells, defensins, and the commensal microbiota: a hypothesis on intimate interplay at the intestinal mucosa. Semin. Immunol. 19:70–83.
22. Sartor, R. B. 2006. Mechanisms of disease: pathogenesis of Crohn's disease and ulcerative colitis. Nat. Clin. Pract. Gastroenterol. Hepatol. 3:390–407.
23. Sartor, R. B. 2004. Therapeutic manipulation of the enteric microflora in inflammatory bowel diseases: antibiotics, probiotics, and prebiotics. Gastroenterology 126:1620–1633.
24. Schlee, M., J. Wehkamp, A. Altenhoefer, T. A. Oelschlaeger, E. F. Stange, and K. Fellermann. 2007. Induction of human beta-defensin 2 by the probiotic *Escherichia coli* Nissle 1917 is mediated through flagellin. Infect. Immun. 75:2399–2407.
25. Schultz, M., U. G. Strauch, H. J. Linde, S. Watzl, F. Obermeier, C. Gottl, N. Dunger, N. Grunwald, J. Scholmerich, and H. C. Rath. 2004. Preventive effects of *Escherichia coli* strain Nissle 1917 on acute and chronic intestinal inflammation in two different murine models of colitis. Clin. Diagn. Lab Immunol. 11:372–378.
26. Spöttl, T., M. Hausmann, M. Kreutz, A. Peuker, D. Vogl, J. Scholmerich, W. Falk, R. Andreesen, T. Andus, H. Herfarth, and G. Rogler. 2001. Monocyte differentiation in intestine-like macrophage phenotype induced by epithelial cells. J. Leukoc. Biol. 70:241–251.
27. Sturm, A., K. Rilling, D. C. Baumgart, K. Gargas, T. Abou-Ghazale, B. Raupach, J. Eckert, R. R. Schumann, C. Enders, U. Sonnenborn, B. Wiedenmann, and A. U. Dignass. 2005. *Escherichia coli* Nissle 1917 distinctively modulates T-cell cycling and expansion via toll-like receptor 2 signaling. Infect. Immun. 73:1452–1465.
28. Sutherland, L., J. Singleton, J. Sessions, S. Hanauer, E. Krawitt, G. Rankin, R. Summers, H. Mekhjian, N. Greenberger, M. Kelly, et al. 1991. Double blind, placebo controlled trial of metronidazole in Crohn's disease. Gut 32:1071–1075.
29. Taurog, J. D., S. D. Maika, W. A. Simmons, M. Breban, and R. E. Hammer. 1993. Susceptibility to inflammatory disease in HLA-B27 transgenic rat lines correlates with the level of B27 expression. J. Immunol. 150:4168–4178.
30. Wehkamp, J., K. Fellermann, K. R. Herrlinger, C. L. Bevins, and E. F. Stange. 2005. Mechanisms of disease: defensins in gastrointestinal diseases. Nat. Clin. Pract. Gastroenterol. Hepatol. 2:406–415.
31. Wehkamp, J., J. Harder, K. Wehkamp, B. Wehkamp-von Meissner, M. Schlee, C. Enders, U. Sonnenborn, S. Nuding, S. Bengmark, K. Fellermann, J. M. Schroder, and E. F. Stange. 2004. NF-κB- and AP-1-mediated induction of human beta defensin-2 in intestinal epithelial cells by *Escherichia coli* Nissle 1917: a novel effect of a probiotic bacterium. Infect. Immun. 72:5750–5758.

Editor: R. P. Morrison

GASTROENTEROLOGY 2008;134:481–490

Exacerbating Role of γδ T Cells in Chronic Colitis of T-Cell Receptor α Mutant Mice

MASANOBU NANNO,[*] YASUYOSHI KANARI,[‡] TOMOAKI NAITO,[§,‖] NAGAMU INOUE,[¶] TADAKAZU HISAMATSU,[¶] HIROSHI CHINEN,[¶] KEN SUGIMOTO,[#,**] YASUYO SHIMOMURA,[#,**] HIDEO YAMAGISHI,[†] TETSUO SHIOHARA,[††] SATOSHI UEHA,[§§] KOUJI MATSUSHIMA,[§§] MAKOTO SUEMATSU,[‖] ATSUSHI MIZOGUCHI,[#,**] TOSHIFUMI HIBI,[¶] ATUL K. BHAN,[#,**] and HIROMICHI ISHIKAWA[§]

[*]Yakult Central Institute for Microbiological Research, Tokyo; [‡]Department of Biophysics, Graduate School of Science, Kyoto University, Kyoto; [§]Department of Microbiology and Immunology, Keio University School of Medicine, Tokyo; [‖]Department of Biochemistry and Integrative Medical Biology, Keio University School of Medicine, Tokyo; [¶]Department of Internal Medicine, Keio University School of Medicine, Tokyo, Japan; [#]Center for the Study of Inflammatory Bowel Disease, Massachusetts General Hospital, Boston; [**]Department of Pathology, Massachusetts General Hospital, Boston, Massachusetts; [††]Department of Dermatology, Kyorin University School of Medicine, Tokyo, Japan; and [§§]Department of Molecular Preventive Medicine, Graduate School of Medicine, University of Tokyo, Tokyo, Japan

Background & Aims: **T-cell receptor (TCR) γδ T cells are an important component of the mucosal immune system and regulate intestinal epithelial homeostasis. Interestingly, there is a significant increase in γδ T cells in the inflamed mucosa of patients with ulcerative colitis (UC). However, the role of γδ T cells in chronic colitis has not been fully identified.** ***Methods:*** **TCRα-deficient mice, which spontaneously develop chronic colitis with many features of human UC including an increase in γδ T-cell population, represent an excellent model to investigate the role of γδ T cells in UC-like colitis. To identify the role of γδ T cells in this colitis, we herein have generated TCRγ-deficient mice through deletion of all TCR Cγ genes (Cγ1, Cγ2, Cγ3, and Cγ4) using the Cre/*loxP* site-specific recombination system and subsequently crossing these mice with TCRα-deficient mice.** ***Results:*** **An increase in colonic γδ T cells was associated with the development of human UC as well as UC-like disease seen in TCRα-deficient mice. Interestingly, the newly established TCRα$^{-/-}$ × TCRγ$^{-/-}$ double mutant mice developed significantly less severe colitis as compared with TCRα-deficient mice. The suppression of colitis in TCRα$^{-/-}$ × TCRγ$^{-/-}$ double mutant mice was associated with a significant reduction of proinflammatory cytokine and chemokine productions and a decrease in neutrophil infiltration.** ***Conclusions:*** **γδ T cells are involved in the exacerbation of UC-like chronic disease. Therefore, γδ T cells may represent a promising therapeutic target for the treatment of human UC.**

T cell receptor (TCR) γδ T cells are an evolutionary conserved T-cell subset with characteristic properties.[1] TCRγδ-bearing murine dendritic epidermal T cells are involved in the regulation of epidermal integrity and promote wound repair of the skin,[2] whereas intestinal intraepithelial γδ T cells (γδ-IEL) regulate intestinal epithelial homeostasis.[3,4] Recent evidence suggests that γδ T cells are also important in immune surveillance of the epithelium by providing a first line of defense against infectious pathogens attacking the surfaces of the body and in the regulation of linking of innate and acquired immunity.[1,5] Furthermore, γδ T cells appear to down-regulate αβ T cell-driven robust immune responses that often result in severe immunopathology.[1]

The incidence of inflammatory bowel diseases (IBD), namely ulcerative colitis (UC) and Crohn's disease (CD), has increased markedly in recent years. The factors including genetic predisposition, environmental conditions, and aberrant immune response driven by normal intestinal flora are vital for the development and persistence of the inflammatory process.[6,7] In the present study, we aimed at elucidating the role of γδ T cells in the pathogenesis of IBD because there is growing evidence supporting that γδ T cells play an active multifaceted immunoregulatory role in the coordinated innate and acquired immune responses that maintain the integrity of epithelial tissues[1,2,4,5,8] and an increase in γδ T cells in the diseased mucosa has been documented in UC patients.[9,10] In acute colitis induced by administration of either 2,4,6-trinitrobenzene sulfonic acid[11,12] or dextran sulfate sodium,[13,14] a protective role of γδ T cells has been demonstrated. However, the role of γδ T cells in chronic intestinal inflammation resembling UC has not yet been investigated. TCRα$^{-/-}$ (α$^{-/-}$) mice spontaneously develop chronic colitis with several features of human UC including a significant increase in γδ T cells.[15] To illuminate the role of γδ T cells in the pathogenesis of UC-like colitis in α$^{-/-}$ mice, we generated TCRγ$^{-/-}$

Abbreviations used in this paper: **α$^{-/-}$, TCRα$^{-/-}$; ARP, anorectal prolapse; γ$^{-/-}$, TCRγ$^{-/-}$; γδ T cells, TCR γδ T cells; IBD, inflammatory bowel disease; IEL, intestinal intraepithelial T lymphocytes; LP, lamina propria; TCR, T-cell receptor; UC, ulcerative colitis.**

0016-5085/08/$34.00
doi:10.1053/j.gastro.2007.11.056

($\gamma^{-/-}$) mice and examined the severity of colitis in $\alpha^{-/-}$ mice that are genetically engineered to lack γδ T cells.

Materials and Methods

Mice

We newly generated $\gamma^{-/-}$ mice and crossed with $\alpha^{-/-}$ mice[16] to develop double mutant ($\alpha^{-/-} \times \gamma^{-/-}$) mice. The generations of these mice are described in Supplementary Materials (see Supplemental Materials online at www.gastrojournal.org). All mice used were of C57BL/6 (B6) background. The mice were maintained under specific pathogen-free conditions, and all animal procedures described in this study were performed in accordance with the guidelines for animal experiments of Keio University School of Medicine, Yakult Central Institute for Microbiological Research, Kinki University School of Medicine, and Massachusetts General Hospital.

Flow Cytometry and Immunohistochemical Procedures

Methods for isolation of intestinal intraepithelial T cells (IEL) from mouse small intestines and lamina propria (LP) cells from mouse and human large intestines are described in Supplementary Materials. Procedures of cell staining for flow cytometric and immunohistochemical analyses are also described in Supplementary Materials (see Supplemental Materials online at www.gastrojournal.org).

Histologic Evaluation of Colitis

The disease score of colitis (0–10) was estimated in a blind fashion using previously described criteria, namely, a combination of both gross and histologic findings.[17] The gross score was rated as 0, presence of normal beaded appearance; 1, absence of beaded appearance of colon; 2, focally thickened colon; and 3, marked thickness of entire colon. The histologic score was based on the extent of intestinal wall thickening (0–3), inflammatory cell infiltration into LP (0–3), and presence (0 or 1) of ulceration.

Real-Time Reverse-Transcription Polymerase Chain Reaction Analysis

Total RNA was extracted from half of the frozen colonic tissue obtained from each one of wild-type (WT), $\gamma^{-/-}$, $\alpha^{-/-}$, and $\alpha\gamma^{-/-}$ littermate mice, and complementary DNA (cDNA) was prepared. Quantitative real-time reverse-transcription polymerase chain reaction (RT-PCR) was conducted to assess the expression level of TNF-α, IL-1β, IL-6, TGF-β, IFN-γ, IL-7, IL-10, IL-12, KC, MIP-2, GCP-2, MCP-1, MIP-1α, MIP-1β, and HPRT genes using TaqMan probes (Applied Biosystems, Foster City, CA). The relative expression level of genes of interest was normalized to the HPRT gene expression. The detailed procedures are described in Supplementary Materials (see Supplemental Materials online at www.gastrojournal.org).

Measurement of Cytokines and Chemokines by Enzyme-Linked Immunosorbent Assay

Proteins were extracted from the above-described half of the frozen colonic tissue obtained from each one of WT, $\gamma^{-/-}$, $\alpha^{-/-}$, and $\alpha\gamma^{-/-}$ littermate mice. In brief, frozen colonic tissue was homogenized with a sonicator (Ultrasonic Disruptor UD-201, TOMY, Tokyo, Japan) in 5 mL lysis buffer (50 mmol/L Tris-HCl, pH 7.4, 150 mmol/L NaCl, 1% NP-40, 1 mmol/L dithiothreitol, 1 mmol/L EDTA, 1 mmol/L NaF, 1 mmol/L sodium orthovanadate, and complete, Mini EDTA-free proteinase inhibitor [Roche Applied Science, Mannheim, Germany]), the homogenate was clarified by centrifugation at 14,000 rpm for 10 minutes, and the supernatant was subjected to OptEIA ELISA (BD Biosciences, San Diego, CA) for detection of tumor necrosis factor (TNF)-α, interleukin (IL)-1β, and IL-6 and to DuoSet ELISA (R&D Systems, Minneapolis, MN) for detection of transforming growth factor (TGF)-β, interferon (IFN)-γ, keratinocyte-derived chemokine (KC), macrophage inflammatory protein (MIP)-2 and granulocyte chemotactic protein (GCP)-2. Levels in the supernatants were standardized to the total amount of protein in the same supernatants assessed by RC DC Protein Assay (Bio-Rad Laboratories, Hercules, CA).

Chemotaxis Assay

The assays were performed using the ChemoTx 96-well plate No. 101-3 (NeuroProbe, Gaithersburg, MD). Briefly, bone marrow cells collected from femurs, tibias, and humerus of WT mice were recovered by centrifugation at the interphase of 44% and 70% Percoll solutions. Subsequently, 2.5×10^5 bone marrow cells were loaded onto the membrane plate and placed on a flat-bottomed, 96-well microtiter plate containing the colon extracts (0.7 mg protein/mL) from WT, $\alpha^{-/-}$, and $\alpha\gamma^{-/-}$ mice in addition to serially diluted MIP-2 and MCP-1 (R&D Systems). To identify the neutrophils and monocytes, bone marrow cells were labeled with fluorescent dye conjugated monoclonal antibodies (mAb) to Mac-1 and Ly-6C before the assay. After incubation at 37°C for 2 hours, the number of Mac-1$^+$Ly-6C^{low} neutrophils[18] and Mac-1$^+$Ly-6C^{high} monocytes[18] that migrated into the lower wells was determined by a flow cytometry.

Cell Transfer

γδ T cells were purified from the mesenteric lymph nodes (MLNs) and colon of $\alpha^{-/-}$ mice through MACS system, and 2×10^6 purified cells were intravenously transferred twice into $\alpha\gamma^{-/-}$ mice (n = 16) at 4 and 5 months of age. As control group, phosphate-buffered saline (PBS) was intravenously administrated into $\alpha\gamma^{-/-}$ mice (n = 15). The recipient mice were then killed at 6 months of age.

Statistical Analysis

The statistical difference was determined by 2-sided Student *t* test. For the statistical analysis of cell infiltration into the large intestine, 2-sided Mann-Whitney *U* test was used. Difference with $P < .05$ was considered significant.

Results

Generation of TCRγ-Deficient Mice

To begin with, we initially confirmed that γδ T cells were increased in the lymphoid cells isolated from the inflamed colonic mucosa of UC patients as compared with those from the unaffected colonic mucosa of patients with colon cancer (Figure 1*A* and *B*) and also in the lymphoid cells isolated from the inflamed colonic LP of $\alpha^{-/-}$ mice as compared with those from normal colonic LP of age-matched WT littermate mice (Figure 1*C* and *D*).

Precise appreciation of the role of γδ T cells in pathogenesis of colitis in $\alpha^{-/-}$ mice requires the generation of $\alpha^{-/-}$ mice deficient in γδ T cells. However, the previously generated TCRδ$^{-/-}$ ($\delta^{-/-}$) mice[19] lacking γδ T cells could not be used for this purpose because of the genomic localization of TCRδ coding segments within the *V* and *J* segments of TCRα gene.[20] To overcome this difficulty, we newly generated TCRγ$^{-/-}$ mice by disrupting the genes encoding TCR Cγ1, 2, 3, and 4 (CγΔ) using the Cre/*loxP* site-specific recombination system shown in Figure 2. The targeting vector pCγ4ΔNL carrying a *loxP*-flanked *pgk-neo* gene cassette in place of exon 1 of the Cγ4 gene (Figure 2*A*) was introduced into the embryonic stem (ES) clone Vγ6ΔL carrying the allele in which the Vγ6 region was replaced by a single *loxP* site (Figure 2*B*). Transfected cells were cultured in the presence of G418, and G418-resistant recombinant clones showing the joint transmission of Vγ6ΔL and Cγ4ΔNL genes were selected. These ES clones, including the clones carrying both transgenes on the same chromosome, Vγ6ΔL-Cγ4ΔNL (Figure 2*C*), were injected into B6 blastocysts. The chimeric mice obtained were crossed to the CAG-*cre* transgenic B6 mice to generate the Cγ1-, 2-, 3-, and 4-depleted TCRγ-deficient (CγΔ) allele (Figure 2*C*) by *cre*-mediated recombination in F_1 mice during embryonic development.

Subsequently, these F_1 mice were intercrossed to produce homozygous (γ$^{-/-}$) mice (Figure 2*D*), and these mutant γ$^{-/-}$ mice were backcrossed 8 times to B6 mice to obtain γ$^{-/-}$ mice carrying the B6 background. WT ($\alpha^{+/-} \times \gamma^{+/-}$), γ$^{-/-}$ ($\alpha^{+/-} \times \gamma^{-/-}$), $\alpha^{-/-}$ ($\alpha^{-/-} \times \gamma^{+/-}$), and αγ$^{-/-}$ ($\alpha^{-/-} \times \gamma^{-/-}$) littermate F_2 mice were then produced by intercrossing $\alpha^{-/-}$ mice[16] with γ$^{-/-}$ mice. Flow cytometric analysis of IEL from the small intestine confirmed that γδ T cells were absent in γ$^{-/-}$ and αγ$^{-/-}$ mice (Figure 2*E*).

Pathogenic Role of γδ T Cells in UC-Like Colitis

Histologic examination of the colons from 20- to 32-week-old $\alpha^{-/-}$ and αγ$^{-/-}$ mice revealed that inflam-

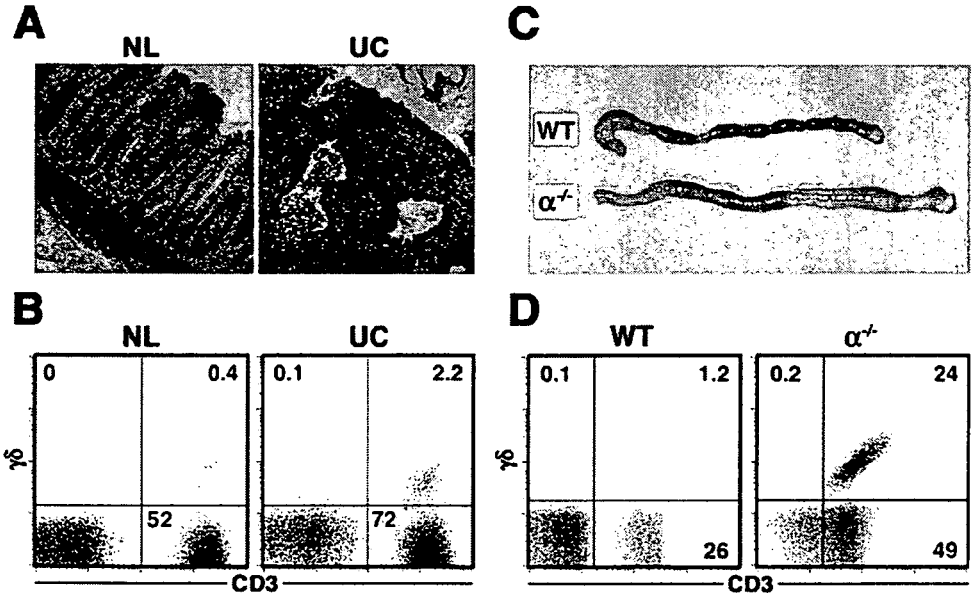

Figure 1. γδ T cells concentrate in the inflamed colonic mucosa of UC patients and colonic LP of $\alpha^{-/-}$ mice suffering from spontaneous chronic colitis. (*A*) A representative colonic tissue section from an ulcerative colitis (*UC*) patient shows a marked infiltration of lymphomyeloid cells, mucosal distortion, crypt abscess, and depletion of goblet cells compared with a normal colonic tissue section (*NL*) (original magnification, ×100). (*B*) A flow cytometry shows increased γδ T-cell population in a diseased colonic LP of UC patient compared with that in a normal colonic LP. This is a representative result of 3 UC patients. (*C*) Large intestines from wild-type (*WT*) mice and $\alpha^{-/-}$ mice suffering from spontaneous chronic colitis are shown. (*D*) A flow cytometry shows increased γδ T-cell population in a diseased colonic LP of $\alpha^{-/-}$ mice compared with that in colonic LP of WT littermate.